Theory of Resonance Suppression in Vibrational Polariton Chemistry

Sebastian Montillo Vega,[1,*] Wenxiang Ying,[1,*] and Pengfei Huo[1,2,†]

[1] *Department of Chemistry, University of Rochester, Rochester, New York 14627, USA*
[2] *Institute of Optics, Hajim School of Engineering, University of Rochester, Rochester, New York 14627, USA*

Recent experiments have demonstrated that it is possible to modify ground-state chemical reactivities by placing an ensemble of molecules in an optical microcavity through resonant coupling between the cavity and vibrational degrees of freedom (DOF) of the molecules. This new strategy of vibrational strong coupling (VSC), if feasible, will offer a paradigm shift in synthetic chemistry through cavity-enabled bond-selective chemical transformations. This so-called VSC regime operates in the *absence* of any light source, occurs under the resonance condition when cavity frequency matches the molecular vibrational frequency, and only occurs at the normal incidence when considering in-plane momentum inside a Fabry-Pérot cavity. In this work, we provide a potential mechanism that explains all observed phenomena. Using numerically exact quantum dynamics simulations and an analytic rate theory, we have demonstrated the resonant suppression of the rate constant when coupling the cavity mode to a vibrational spectator mode in a model reaction. Both the analytic theory and the simulations can explain previously observed phenomena, including the non-linear change of the rate constant when increasing Rabi splitting, modification of both reactive enthalpy and entropy, and for a reason why with a very low barrier, there is a lack of the cavity modification. The analytic theory can also explain the normal incidence condition, and collective coupling effects when solvents are collectively coupled to both cavity mode and reaction coordinate.

Recent experiments [1–14] demonstrated that chemical reaction rate constants can be suppressed [1–6, 9, 10] or enhanced [11–14] by resonantly coupling molecular vibrations to quantized radiation modes inside a Fabry-Pérot (FP) microcavity [6, 8, 15]. This effect, known as vibrational strong coupling (VSC) modified chemical reactivity, has the potential to selectively slow down competing reactions [2] or speed up a target reaction, thus achieving mode selectivity and offering a paradigm shift in chemistry. For example, VSC has been shown to selectively slow down one reaction over a competing reaction and revert the selectivities [2, 16], enabling a new cavity-enabled bond-selective chemical transformation strategies in synthetic chemistry.

There are several characteristic, universal phenomena in the VSC experiments [17, 18], including

(1) The resonance effect [1, 10], where the maximum VSC effect occurs when the cavity frequency is tuned to the vibrational frequency $\omega_c = \omega_Q$.

(2) The normal incidence effect [1], where the VSC effect only happens when the in-plane photon momentum is $k_{\|} = 0$.

(3) The collective effect [1, 4, 11] where the *magnitude* of VSC modification increases when increasing the number of molecules N.

(4) The reaction is under thermal activation without any optical pumping [1, 2].

To the best of our knowledge, there is no unified, microscopic theory that can simultaneously explain all of the above-observed phenomena [17]. Despite extensive theoretical efforts [10, 16, 19–42], the fundamental mechanism and theoretical understanding of the cavity-modified ground-state chemical kinetics remain elusive [17, 18, 43, 44]. There are many insightful hypothesis and mechanisms [10, 16, 19–35, 37–42] that have been proposed to explain the VSC effects. Unfortunately, a clear theoretical understanding of cavity-modified ground-state chemical reactivity remains missing.

Further, there is no analytic rate constant theory that could explain the sharp resonance suppression either (condition 1). Transition state theory (TST) predicts no frequency-dependent VSC effects [22, 25] and existing rate constant theory beyond TST often depends on the barrier frequency [25, 41, 45], or has a very broad cavity-frequency dependence for the rate changes [25, 30, 45]. These shortcomings of using the existing rate theories to explain VSC effects strongly hint that a proper mechanistic description of the VSC resonance suppression leads to a completely new analytic rate constant expression. On the other hand, related to the collective effect, seemingly promising simulations in Ref. 33 showed that the effect of collective resonance enhancement of rate was due to the relaxation rate constant of the non-equilibrium initial condition of the molecule-cavity hybrid system [46], whereas the chemical reaction rate constant remains the same as outside the cavity when the dynamics enter into the linear response regime [46].

There are several key progresses in the past years that could potentially lead to a unified theory and mechanism that explains the observed VSC effects. First, the sharp resonance enhancement (condition 1) will show up when using a quantum state description of the vibrational states, which has been demonstrated with exact quantum dynamics simulation [41, 47], mixed quantum-classical simulations [48], and analytic rate constant theory based

* S.M.V. and W.Y contributed equally to this work.
† pengfei.huo@rochester.edu

https://doi.org/10.26434/chemrxiv-2024-m7t4c **ORCID:** https://orcid.org/0000-0002-8639-9299 Content not peer-reviewed by ChemRxiv. **License:** CC BY 4.0

on Fermi's golden rule [47, 49, 50]. Second, using the photonic density of states (DOS) analysis and the FGR rate expression that explicitly accounts for the in-plane effective photonic lifetime, the normal incidence condition (condition 2) can be rationalized [49, 50]. Third, it has been shown that when the N solvent vibrations couple to both cavity mode and a reaction coordinate, the collective effect (condition 3) will naturally emerge [29], although the resonance condition in Ref. 29 was not $\omega_c = \omega_Q$ due to the use of a classical rate theory which is not sensitive to ω_Q but rather to the reaction barrier frequency [25] (or more generally speaking, curvatures of the reaction barrier or the partition function that sums over all frequencies). Nevertheless, the solvent-strong coupling could influence the properties of solute molecules as shown in recent experiments [51]. All of the above-mentioned theoretical progress assumes a thermal condition without any laser-pumping excitation of the system (condition 4).

In this work, we integrate our previous success and progress into a unified microscopic mechanism that explains all of the experimentally observed VSC effects, giving the resonance condition [47], the normal incidence condition [49], the collective effect [29], and operating under the thermally activated condition. We consider a theoretical model where cavity mode couples to a set of solvent vibrations $\{\mathcal{Q}_j\}$ (spectator modes, or rate promoting vibrations) which in turn couple to a reaction coordinate R_0. This is a model that captures the essential feature of the recent VSC experiments [10], as well as classical simulations that demonstrate the collective effect for reaction rate constant [29] or vibrational energy relaxation [52]. We use the effective spectral density theory to treat how cavity mode collectively coupled to the spectator modes can influence the forward reaction along a given reaction coordinate R_0, and derive an analytic rate constant expression based on Fermi's Golden Rule (FGR). We further use numerically exact quantum dynamics simulation based on the Hierarchical Equations of Motion (HEOM) approach to verify the accuracy of the theory. We discuss the fundamental mechanism of VSC-suppressed reaction, the basic scaling of VSC effects with light-matter coupling strengths, the null effect, and collective as well as normal incidence conditions.

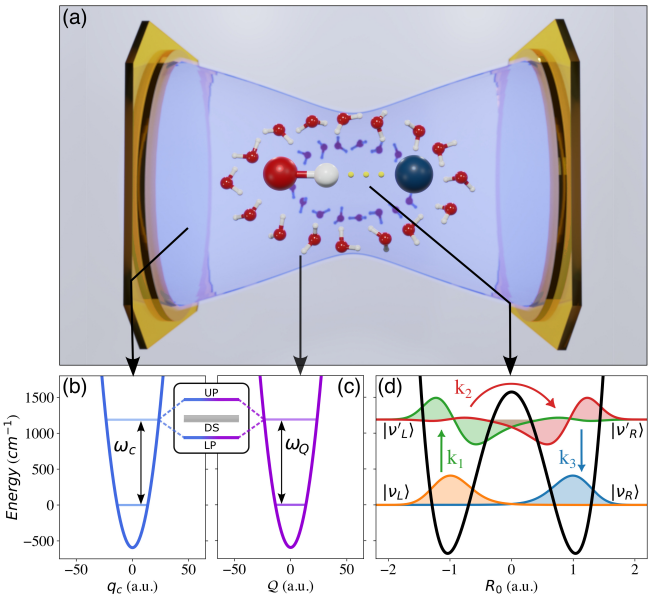

FIG. 1. **Schematic illustration of the VSC-modified reactions and the mechanisms**. (**a**). Schematic illustration of a reactive molecule whose reaction coordinate is coupled to a set of solvent vibrations, which are in turn coupled to a cavity mode. (**b**) Photonic potential coupled to (**c**) an intermolecular vibration whose hybridization leads to a set of polaritonic states with Rabi splitting Ω_R. The intermolecular vibration in turn couples to a reaction coordinate R_0. (**d**) Potential energy surface of the chemical reaction along the reaction coordinate, with four key vibrational states visualized.

RESULTS

Theoretical model. We use the Pauli-Fierz (PF) Hamiltonian to describe the light-matter interaction of molecular vibrations in an optical cavity [18, 53]. In the dipole gauge [53], single mode, long-wavelength approximations [18], the PF Hamiltonian takes the form

$$\hat{H} = \hat{H}_{\rm M} + \hat{H}_{\rm RPV} + \hat{H}_{\rm LM} + \hat{H}_{\nu} + \hat{H}_{\rm loss}, \qquad (1)$$

where $\hat{H}_{\rm M} = \hat{T}_0 + \hat{V}(\hat{R}_0)$ is the Hamiltonian of the reactive molecule whose ground state potential energy surface is taken to be a symmetric double well potential along the reaction coordinate $\hat{R}_0$, see Methods, Eq. 25 for details. We use a set of localized diabatic vibrational states ($|\nu_{\rm L}\rangle, |\nu_{\rm R}\rangle, |\nu'_{\rm L}\rangle, |\nu'_{\rm R}\rangle$) to represent ground and excited vibrational states associated with the left well (reactant) and the right well (product), which are depicted in Fig, 1d. In this picture, the vibrational frequency ω_0 for the reactant is defined as the transition frequency associated with $|\nu_{\rm L}\rangle \rightarrow |\nu'_{\rm L}\rangle$, see Methods, Eqs. 26-28 for details. The description of $\hat{H}_{\nu}$ and $\hat{H}_{\rm loss}$ are provided in Methods, Eqs. 29-31. The rest of the details for the model are provided in Supplementary Note 1.

Condensed phase chemical reactions often possess complex structures, where the reaction coordinate strongly interacts with a variety of environmental vibrations. These fast dynamical modes, known as rate promoting vibrations (RPV), have been recognized as playing a key role in increasing the chemical reaction rate [54–57]. Moreover, it has been theoretically shown [10, 26, 29, 46] that the cavity mode could significantly influence the reaction dynamics when it interacts with one of such RPV or solvent degrees of freedom (DOF). We model the interactions between RPV modes and R_0 using the following Hamiltonian

$$\hat{H}_{\rm RPV} = \sum_{j=1}^{N} \frac{\hat{\Pi}_j^2}{2} + \frac{\omega_{\rm Q}^2}{2}\left(\hat{\mathcal{Q}}_j - \frac{\mathcal{C}_j}{\omega_{\rm Q}^2}\hat{R}_0\right)^2, \qquad (2)$$

https://doi.org/10.26434/chemrxiv-2024-m7t4c **ORCID:** https://orcid.org/0000-0002-8639-9299 Content not peer-reviewed by ChemRxiv. **License:** CC BY 4.0

where $\hat{\Pi}_j$ and $\hat{\mathcal{Q}}_j$ are the momentum and coordinate for the RPV modes, which could be a spectator mode or solvent modes that coupled to R_0 with coupling strength $\mathcal{C}_j$. These modes have a uniform frequency ω_{Q}. Further, we introduce the reorganization energy for R_0 caused by $\mathcal{Q}_j$ coupling, defined as

$$\Lambda = \sum_{j=1}^{N} \mathcal{C}_j^2/(2\omega_{\mathrm{Q}}^2). \tag{3}$$

Note that this is a collective quantity between reaction coordinate R_0 and the solvent DOF $\mathcal{Q}_j$. For the solvent-solute interactions in Eq. 2, with an increasing number of solvent molecules, the outer sphere solvents will only be weakly coupled to the solute, while the inner sphere solvent strongly coupled to the solute, resulting in a solute-solvent distance-specific coupling strength $\mathcal{C}_j$. In this study, we keep Λ as a fixed parameter.

The light-matter interaction Hamiltonian $\hat{H}_{\mathrm{LM}}$ considers one cavity mode coupled to the $\{\mathcal{Q}_j\}$ modes, expressed as

$$\hat{H}_{\mathrm{LM}} = \frac{\hat{p}_{\mathrm{c}}^2}{2} + \frac{\omega_{\mathrm{c}}^2}{2}\left(\hat{q}_{\mathrm{c}} + \sqrt{\frac{2}{\omega_{\mathrm{c}}}}\eta_{\mathrm{c}} \sum_{j=1}^{N} \hat{\mathcal{Q}}_j \cdot \cos\varphi_j\right)^2, \tag{4}$$

where the photonic position operator $\hat{q}_{\mathrm{c}} = \sqrt{\hbar/(2\omega_{\mathrm{c}})}(\hat{a}^\dagger + \hat{a})$ and momentum operator $\hat{p}_{\mathrm{c}} = i\sqrt{\hbar\omega_{\mathrm{c}}/2}(\hat{a}^\dagger - \hat{a})$ are expressed in terms of the photonic creation operator $\hat{a}^\dagger$ and annihilation $\hat{a}$ for a given cavity mode, with ω_{c} as the cavity frequency. A generalization of this term with many cavity modes will be discussed at the end of the paper. Further, η_{c} is the light-matter coupling strength expressed as follows [18]

$$\eta_{\mathrm{c}} = \sqrt{\frac{1}{2\hbar\omega_{\mathrm{c}}\epsilon_0\mathcal{V}}}, \tag{5}$$

where ϵ_0 is the permittivity inside the cavity, and $\mathcal{V}$ is the effective quantization volume of that mode. For simplicity, we have assumed that the dipole operators are linear [24, 41] such that $\hat{\boldsymbol{\mu}}(\mathcal{Q}_j)\cdot\hat{\mathbf{e}}_\perp \approx \hat{\mathcal{Q}}_j \cdot \cos\varphi_j$, where $\hat{\mathbf{e}}_\perp$ is the transverse field polarization direction. In contrast to the $R_0 - \mathcal{Q}_j$ interaction characterized by $\mathcal{C}_j$ (electrostatic interactions) which depends on the solute-solvent distance, the cavity mode, on the other hand, interacts with all solvent modes $\{\mathcal{Q}_j\}$ with η_{c} weighted by $\cos\varphi_j$, resulting in delocalized interactions that can be observed from the Rabi splitting from spectroscopy [58].

Under the resonance condition of $\omega_{\mathrm{c}} = \omega_{\mathrm{Q}}$, the total Rabi splitting from the spectral measurements is related to the light-matter coupling strength. When there is no dipole angle disorder ($\cos\varphi_j = 1$ for all j), the Rabi splitting is expressed as [17, 18, 58, 59]

$$\Omega_{\mathrm{R}} = 2\sqrt{N}\eta_{\mathrm{c}}\omega_{\mathrm{c}}\mu_{\mathrm{Q}} = \sqrt{2N\omega_{\mathrm{c}}}\eta_{\mathrm{c}} = \sqrt{\frac{N}{\epsilon_0\mathcal{V}}} \tag{6}$$

where the transition dipole matrix element associated with $\mathcal{Q}_j$ is expressed as $\mu_{\mathrm{Q}} = \langle 0|\hat{\mathcal{Q}}_j|1\rangle = \sqrt{1/(2\omega_{\mathrm{Q}})}$ which is assumed to be identical for all $\mathcal{Q}_j$ modes.

Analytic Rate Theory. Under the thermally activated initial condition, the reaction coordinate R_0 undergoes a barrier-crossing process, reaches the transition state, and finally relaxes to the product configuration. This is the well-accepted classical mechanism that can be properly described by transition state theory. Quantum mechanically, the same process is described as (1) the thermally activated vibrational excitation on the reactant side $|\nu_{\mathrm{L}}\rangle \to |\nu'_{\mathrm{L}}\rangle$, (2) vibrational excited states transition $|\nu'_{\mathrm{L}}\rangle \to |\nu'_{\mathrm{R}}\rangle$, and (3) vibrational relaxation on the product side $|\nu'_{\mathrm{R}}\rangle \to |\nu_{\mathrm{R}}\rangle$. The population dynamics from the HEOM exact simulations (see Supplementary Note 2 and 3) indicate that the reaction mechanism can be described as follows [47]

$$|\nu_{\mathrm{L}}\rangle \xrightarrow{k_1} |\nu'_{\mathrm{L}}\rangle \xrightarrow{k_2} |\nu'_{\mathrm{R}}\rangle \xrightarrow{k_3} |\nu_{\mathrm{R}}\rangle\,, \tag{7}$$

where the initial vibrational excitation ($|\nu_{\mathrm{L}}\rangle \to |\nu'_{\mathrm{L}}\rangle$) is the rate-limiting step, such that $k_1 \ll k_2, k_3$, see Fig. 1d. This will lead to a steady state population (time-independent plateau population) of the intermediate states $|\nu'_{\mathrm{L}}\rangle$ and $|\nu'_{\mathrm{R}}\rangle$, and the overall rate constant for the entire reaction (k) can be approximate as $k \approx k_1$. The $|\nu_{\mathrm{L}}\rangle \to |\nu'_{\mathrm{L}}\rangle$ transition is influenced by the energy exchange between the phonon bath and the RPV modes $\{\mathcal{Q}_j\}$. When resonantly coupled to the cavity, the light-matter hybrid system has a set of polaritonic modes with frequencies $\omega_\pm = \omega_{\mathrm{Q}} \pm \Omega_{\mathrm{R}}/2$, thus effectively removing the RPV's from the $|\nu_{\mathrm{L}}\rangle \to |\nu'_{\mathrm{L}}\rangle$ transition, explicitly changing the value of k_1, and as $|\nu_{\mathrm{L}}\rangle \to |\nu'_{\mathrm{L}}\rangle$ is still the rate-limiting step for system compiled inside the cavity (see Supplementary Note 4), the influence of cavity on k_1 explicitly shows up in the entire apparent rate constant of the reaction.

Based on this observation, the impact of VSC on the rate is solely attributed to the cavity interacting with the RPV modes, and influencing the rate constant of the $|\nu_{\mathrm{L}}\rangle \to |\nu'_{\mathrm{L}}\rangle$ transition, hence imprint its impact on the apparent rate constant of the reaction. The overall constant is expressed as $k \approx k_1 = k_{\mathrm{D}} + \alpha \cdot k_{\mathrm{VSC}}$, where k_{D} is the rate constant for the double-well potential without coupling to any RPV modes $\mathcal{Q}_j$ or the cavity mode q_{c}, and α is a scaling parameter. When FGR is exact and the role of $\{\mathcal{Q}_j\}$ and q_{c} are directly additive to k, $\alpha = 1$. For the previous work of VSC-enhanced rate constant studies, we found [47, 49] that $\alpha \in [0.5, 1]$ are needed to bring a quantitative agreement of the FGR expression with the numerically exact results. Throughout the paper, we report the ratio of the rate constant inside and outside the cavity as follows

$$k/k_0 = k_{\mathrm{D}}/k_0 + \alpha \cdot k_{\mathrm{VSC}}/k_0, \tag{8}$$

where k_0 and k_{D} are directly obtained from HEOM simulations as they are not related to the coupling of the cavity mode. In this work, under the condition $\eta_{\mathrm{c}} = 0$ (outside the cavity), we find that $\alpha \approx 0.7$ will bring the FGR analytic results to quantitatively agree with the numerically exact results from HEOM. This parameter is

https://doi.org/10.26434/chemrxiv-2024-m7t4c **ORCID:** https://orcid.org/0000-0002-8639-9299 Content not peer-reviewed by ChemRxiv. **License:** CC BY 4.0

then fixed for all cases of η_c when coupling the RPV mode to the cavity.

We aim to develop an analytic rate constant theory that describes the role of $\{\mathcal{Q}_j\}$ and q_c on the rate constant. To this end, we derived an effective spectral density, $J_{\text{eff}}(\omega)$, that describes the coupling of $\hat{H}_{\text{RPV}}+\hat{H}_{\text{LM}}+\hat{H}_{\text{loss}}$ to the reaction coordinate R_0, based on the effective spectral density theory [60, 61]. The details of the derivation are provided in Supplementary Note 5, and the most general expression is provided in Eq. 34 in **Method**. A more insightful, approximate expression is

$$J_{\text{eff}}(\omega) = \frac{\Lambda \cdot \omega_{\text{Q}}^2 \cdot \omega\Gamma_{\text{Q}}(\omega)}{\left[\omega_{\text{Q}}^2 - \omega^2 + \tilde{\mathcal{R}}(\omega)\right]^2 + (\omega\Gamma_{\text{Q}}(\omega))^2}, \quad (9)$$

where Λ (defined in Eq. 3) characterizes the couplings between N RPV modes (*e.g.*, solvent DOF) $\{\mathcal{Q}_j\}$ with R_0, and ω_{Q} is the solvent frequency which we assume to be identical for all $\{\mathcal{Q}_j\}$. In addition, Γ_{Q} characterizes the excitation decay rate in the $\{\mathcal{Q}_j\}$ modes

$$\Gamma_{\text{Q}}(\omega) = \frac{2\lambda_{\text{Q}}}{\gamma_{\text{Q}}} + \frac{2N\chi^2 \cdot \omega_{\text{c}}^3\eta_{\text{c}}^2\tau_{\text{c}}^{-1}}{\left(\omega_{\text{c}}^2 - \omega^2\right)^2 + \omega^2\tau_{\text{c}}^{-2}}, \quad (10)$$

where λ_{Q} and γ_{Q} are phonon bath parameters for $\{\mathcal{Q}_j\}$ modes (see Eq. 30b), τ_{c} is the cavity lifetime, and ω_{c} is the cavity frequency for mode q_{c}. Further, χ characterizes the angle of the vibrational dipole operator relative to the cavity mode q_{c}, with the following expression

$$\chi = \frac{1}{N}\sum_j \cos\varphi_j \equiv \langle\cos\varphi\rangle, \quad (11)$$

Finally, $\tilde{\mathcal{R}}(\omega)$ in Eq. 9 is expressed as

$$\tilde{\mathcal{R}}(\omega) = \frac{2N\chi^2 \cdot \omega_{\text{c}}\eta_{\text{c}}^2\omega^2}{\left(\omega_{\text{c}}^2 - \omega^2\right)^2 + \omega^2\tau_{\text{c}}^{-2}} \cdot (\omega^2 - \omega_{\text{c}}^2 + \tau_{\text{c}}^{-2}). \quad (12)$$

Note that in this approximate form of $J_{\text{eff}}(\omega)$ in Eq, 9, there are $N-1$ dark states that do not appear [62], thus being decoupled [29] from the reaction coordinate $\hat{R}_0$. This is due to a mean-field-like approximation for the $\mathcal{C}_j$ when deriving Eq. 9. In the general expression of the spectral density (Eq. 34), the dark states can still show up when having the angle and coupling disorders, but the dark-state peak magnitude does not dominate when considering a certain range of disorders. This will be discussed in detail in the **Collective coupling mechanism** section.

Fig. 2a presents $J_{\text{eff}}(\omega)$ at various Ω_{R}. At $\Omega_{\text{R}} = 0$ (black curve), the peak of $J_{\text{eff}}(\omega)$ is located at the frequency of ω_{Q}, and the RPV effect is at its maximum due to $\omega_{\text{Q}} = \omega_0$. With the higher Ω_{R}, $J_{\text{eff}}(\omega)$ split into two peaks (corresponding to the two vibrational polariton frequencies $\omega_\pm \approx \omega_{\text{Q}} \pm \Omega_{\text{R}}/2$), and is moving away from ω_0, hence reduce the RPV effect and the value of k_1 for $|\nu_{\text{L}}\rangle \to |\nu'_{\text{L}}\rangle$ transition (c.f. Eq. 7). Note that the $J_{\text{eff}}(\omega)$ expression is only sensitive to the collective coupling strength Ω_{R}, and for $N > 1$, the behavior of $J_{\text{eff}}(\omega)$ is identical to $N = 1$ as long as Ω_{R} and Λ are identical. The rest of the dark vibrational modes are decoupled from q_{c} and will not explicitly show up in $J_{\text{eff}}(\omega)$.

To evaluate the $|\nu_{\text{L}}\rangle \to |\nu'_{\text{L}}\rangle$ transition rate constant k_{VSC} (Eq. 8), we use the FGR

$$\kappa(\omega) = 2|\Delta_x|^2 \cdot J_{\text{eff}}(\omega) \cdot n(\omega), \quad (13)$$

where ω is the transition frequency, $\Delta_x = \langle\nu_{\text{L}}|\,\hat{R}_0\,|\nu'_{\text{L}}\rangle$ the vibrational transition dipole for the $|\nu_{\text{L}}\rangle \to |\nu'_{\text{L}}\rangle$ transition, and

$$n(\omega) = 1/(e^{\beta\omega} - 1) \quad (14)$$

is the Bose-Einstein distribution function, $\beta \equiv 1/(k_{\text{B}}T)$ is the inverse of temperature T, and k_{B} is the Boltzmann constant. Note that the validity of FGR is under the condition $\sqrt{\Lambda\omega_{\text{Q}}} \cdot |\Delta_{\text{x}}| \ll k_{\text{B}}T \approx 200\ \text{cm}^{-1}$ under $T = 300$ K, and the "strong coupling condition" [63] will not break the validity of FGR (although for all known VSC-induced chemistry experiments, $\Omega_{\text{R}} = 100\ \text{cm}^{-1}$). In this work, the model system has $\sum_j^N \mathcal{C}_j \cdot |\Delta_{\text{x}}|/\sqrt{2\omega_{\text{Q}}} \approx 10\ \text{cm}^{-1}$.

For the fixed energy level between $|\nu_{\text{L}}\rangle$ and $|\nu'_{\text{L}}\rangle$ states, the FGR rate constant is expressed as $k_{\text{VSC}} = \kappa(\omega_0)$, where $\hbar\omega_0$ is the energy difference for the transition. However, R_0 also couples to its own solvent bath (see Eq. 29), and has fluctuating energy levels. To account for this effect, we add a broadening function $\mathcal{A}_0(\omega - \omega_0)$ to the frequency ω_0, with a Lorentzian shape [47, 50] (for the case under the homogeneous limit [64]) expressed as

$$\mathcal{A}_0(\omega - \omega_0) = \frac{1}{\pi}\frac{\Gamma_0}{(\omega - \omega_0)^2 + \Gamma_0^2}, \quad (15)$$

with the broadening parameter [47] expressed as $\Gamma_0^2 = (\epsilon_z^2/\pi)\int_0^\infty d\omega\ J_0(\omega)\coth(\beta\omega/2)$, and $\epsilon_z \equiv \langle\nu'_{\text{L}}|\hat{R}_0|\nu'_{\text{L}}\rangle - \langle\nu_{\text{L}}|\hat{R}_0|\nu_{\text{L}}\rangle$. The full VSC modified rate constant should be expressed as a convolution [47] between $\kappa(\omega)$ and $\mathcal{A}_0$ through $k_{\text{VSC}} = \int_0^\infty d\omega\ \kappa(\omega) \cdot \mathcal{A}_0(\omega - \omega_0)$, with detailed expression

$$k_{\text{VSC}} = 2|\Delta_x|^2 \int_0^\infty d\omega \frac{\Lambda\omega_{\text{Q}}^2 \cdot \omega\Gamma_{\text{Q}}(\omega) \cdot \mathcal{A}_0(\omega - \omega_0) \cdot n(\omega)}{\left[\omega_{\text{Q}}^2 - \omega^2 + \tilde{\mathcal{R}}(\omega)\right]^2 + (\omega\Gamma_{\text{Q}}(\omega))^2}, \quad (16)$$

The analytic expression of k_{VSC} in Eq. 16 is the **first key result** of this work.

Under the resonance condition $\omega_{\text{c}} = \omega_{\text{Q}}$ and the the lossless limit $\tau_{\text{c}} \to \infty$, Eq. 9 can be simplified as follows

$$J_{\text{eff}}(\omega) = \frac{\Lambda \cdot \omega\Gamma_{\text{Q}} \cdot (\omega_{\text{Q}}^2 - \omega^2)^2}{[(\omega_{\text{Q}}^2 - \omega^2)^2 - \Omega_{\text{R}}^2\omega^2]^2 + [\omega\Gamma_{\text{Q}} \cdot (\omega_{\text{Q}}^2 - \omega^2)]^2} \quad (17)$$

where $\Gamma_{\text{Q}} = 2\lambda_{\text{Q}}/\gamma_{\text{Q}}$ is frequency independent part of $\Gamma_{\text{Q}}(\omega)$ (c.f. Eq. 10). As the VSC rate constant modification is dependent on $J_{\text{eff}}(\omega)$ (Eq. 13), the theory clearly

https://doi.org/10.26434/chemrxiv-2024-m7t4c **ORCID:** https://orcid.org/0000-0002-8639-9299 Content not peer-reviewed by ChemRxiv. **License:** CC BY 4.0

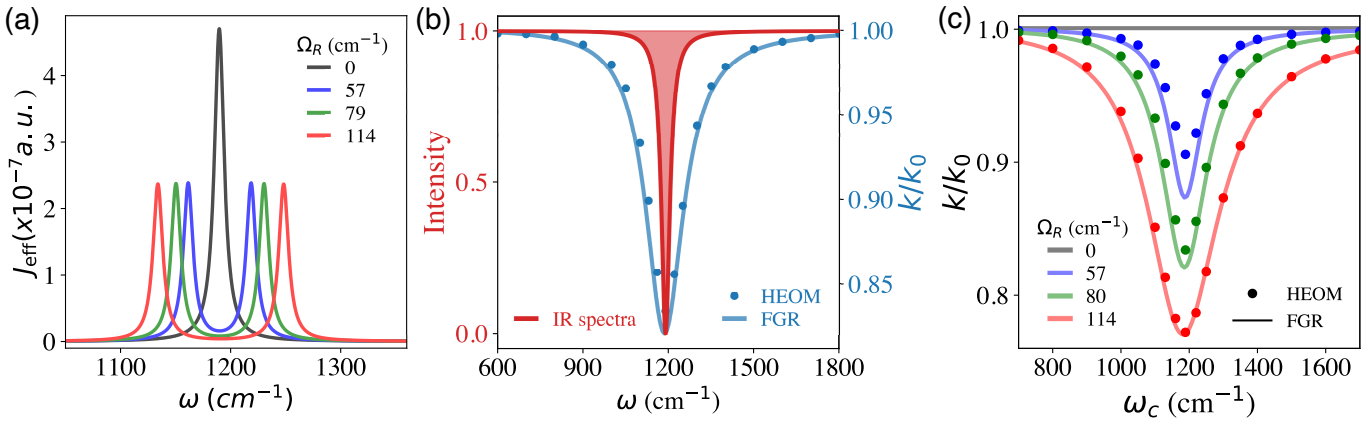

FIG. 2. **Resonance behavior of the VSC effect.** (**a**) Effective spectral density $J_{\rm eff}$ (Eq. 9) with different values of $\Omega_{\rm R}$, where the two peaks correspond to the polariton modes. (**b**) VSC enabled rate constant reduction (blue) and the IR spectra for the spectator mode $\mathcal{Q}_j$ outside the cavity, both of which occur at $\omega_{\rm c} = \omega_{\rm Q}$. The ratio of inside and outside the cavity rate constant k/k_0 obtained from analytic FGR theory (blue solid line) and HEOM (blue solid circles) for $N = 1$ with $\Omega_{\rm R} = 57$ cm^{-1}. (**c**) Normalized rate constant profile k/k_0 (with respect to the outside cavity case k_0) as a function of cavity frequency $\omega_{\rm c}$ and various $\Omega_{\rm R}$. All calculations are done with a cavity lifetime $\tau_{\rm c} = 500$ fs. The FGR results (solid lines) are re-scaled by a factor of $\alpha = 0.7$ (see Eq. 8).

indicates a non-linear dependence of $k_{\rm VSC}$ with collective Rabi splitting $\Omega_{\rm R}$, which has been experimentally observed [4]. Particularly, further simplifications indicate a scaling

$$k_{\rm VSC} \propto \frac{1}{\Omega_{\rm R}^2} \propto \frac{1}{N\eta_{\rm c}^2} \tag{18}$$

In fact, both the HEOM numerical data (Fig. 3a) and the experimental results (*e.g.*, Fig. 3D in Ref. 4) can be fitted well with $k/k_0 = k_D/k_0 + a/(1 + b \cdot \Omega_{\rm R}^2)$ (where a, b are fitting parameters), with details provided in Supplementary Note 6. This scaling relation is the **second key results** of this work.

VSC rate constant modifications. To validate the $k_{\rm VSC}$ theory in Eq. 16, we perform numerical simulations of the rate constants for a single molecule ($N = 1$) coupled to a single cavity mode, where the details are provided in Methods. The parameters used for $\hat{V}(\hat{R}_0)$ set the well frequency $\omega_0 \approx 1189.7$cm^{-1}. For $N = 1$, the RPV mode could be either an intermolecular vibration or a nearby solvent that has a frequency $\omega_{\rm Q} = \omega_0$. Further, we set $\chi = 1$ that corresponds to a vibrational dipole aligned to the cavity mode. All the simulations are performed at $T = 300$ K and a cavity lifetime $\tau_{\rm c} = 500$ fs. The exact quantum dynamics propagation is done by using the hierarchical equations of motion (HEOM) approach [65–68].

Fig. 2b presents the infrared (IR) profile of the RPV mode (red curve), alongside the cavity-dependent rate profile (blue curve) obtained from the HEOM simulations (blue dots) and the FGR approach (blue solid line) outlined in Eq. 8. Both profiles exhibit a distinct sharp peak around $\omega_{\rm Q}$, which is an essential feature observed in most VSC experiments [1, 10]. In particular, existing theories for resonance suppression often have a much broader rate of constant peak (as a function of cavity frequency) that is significantly broader than the width of the lineshape [30, 45]. To the best of our knowledge, Eq. 16 is the **first** analytic theory that is capable of describing a sharp resonance suppression behavior indicated in Fig. 2c.

Fig. 2c presents the cavity frequency dependence of k/k_0. Here, the maximum suppression is achieved when $\omega_c = \omega_{\rm Q}$. The VSC suppression effects are enlarged at a larger $\Omega_{\rm R}$, because the peaks in $J_{\rm eff}(\omega)$ are farther away from the $|\nu_{\rm L}\rangle \rightarrow |\nu'_{\rm L}\rangle$ transition (as can be seen from Fig. 2a). This increase in $\Omega_{\rm R}$ also allows for light-matter interactions at larger cavity detuning, contributing to the broader rate profile. Our analytic FGR expression (Eq. 16) accurately captures the cavity frequency dependence of the rate constants for a wide range of $\Omega_{\rm R}$. As such, $k_{\rm VSC}$ in Eq. 16 has achieved a quantitative agreement with the HEOM simulation results and is capable of describing the sharp resonance behavior observed in the experiments [1, 10].

With the analytic expression of $k_{\rm VSC}$ in Eq. 16, we further explore the behavior of VSC modified rate constant under the resonance condition $\omega_{\rm c} = \omega_{\rm Q}$. We aim to connect with two kinds of experiments. The first kind is the earlier work by Ebbesen and co-worker [1] for a deprotection reaction of alkynyl-silane, as well as the recent work by Simpkins [10] with alcoholysis reaction between phenylisocyanate and cyclohexanol. Both reactions show a resonance suppression captured in Fig. 2. The second kind is the CN radical-hydrogen atom abstraction reaction explored by Weichman and co-workers [69, 70], where there is no explicit VSC effect (null effect).

Fig. 3a presents k/k_0 (blue dots and curve) as a function of $\Omega_{\rm R}$ in the range when the strong coupling condition is achieved. The results are obtained from HEOM simulations (blue dots), as well as from the FGR analytic

https://doi.org/10.26434/chemrxiv-2024-m7t4c **ORCID:** https://orcid.org/0000-0002-8639-9299 Content not peer-reviewed by ChemRxiv. **License:** CC BY 4.0

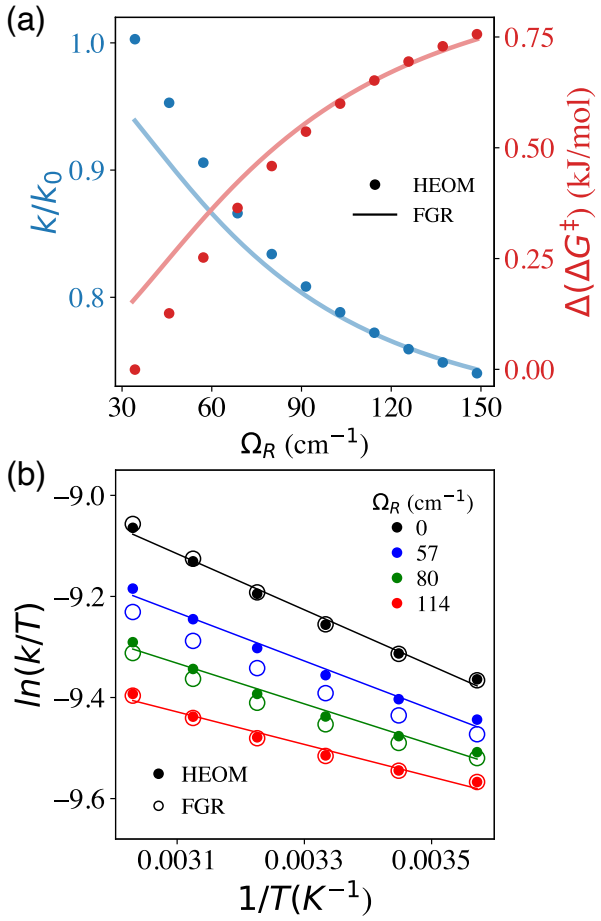

FIG. 3. **VSC modification of the rate constant predicted by FGR theory (Eq. 16).** (**a**) Ratio of the rate constant inside and outside the cavity, k/k_0, and effective free energy barrier change $\Delta(\Delta G^{\ddagger})$ at different Ω_{R}. (**b**) Eyring plot of $\ln(k/T)$ v.s. $1/T$ at various Ω_{R}. In all cases, the cavity is under the resonance condition $\omega_{\mathrm{c}} = \omega_{\mathrm{Q}}$.

expression (blue curve) based on Eq. 8 and Eq. 16. The results clearly show a non-linear relation of the rate constant with the Rabi splitting. In particular, at a large Rabi splitting, the maximum suppression of k/k_0 converges to the value of the bare double rate ($k \to k_{\mathrm{D}}$). As shown in Fig. 2b, the cavity ultimately removes the effects the RPV mode has on the reaction rate by splitting the spectral density and shifting it away from the frequency of ω_0. The trend of k/k_0 closely resembles the experimental trend (*e.g.*, Fig. 3D in Ref. 4), and the FGR analytic expression closely agrees with the HEOM results, especially for a large value of Ω_{R}. The fundamental scaling in Eq. 18 is also observed, with details provided in the Supplemental Note 6.

Fig. 3a also presents the change of the effective free energy barrier $\Delta(\Delta G^{\ddagger})$ (red), directly calculated from the rate constant ratio k/k_0 obtained from HEOM simulations (red dots) and FGR (red line). One can interpret the rate constant changes as the change of the effective free energy barrier $\Delta(\Delta G^{\ddagger})$ through [4, 11, 47] $\Delta(\Delta G^{\ddagger}) = \Delta G^{\ddagger} - \Delta G_0^{\ddagger} = -k_{\mathrm{B}}T \ln(k/k_0)$. Note that this is *not* an actual change in the free-energy barrier, but rather an effective measure of the *purely kinetic* effect. Here, one can see a non-linear relation of $\Delta(\Delta G^{\ddagger})$ with Ω_{R} that agrees with what has been observed experimentally (*e.g.*, Fig. 3C in Ref. 4). Preliminary experimental investigations [4] suggest a non-linear trend between $\Delta(\Delta G^{\ddagger})$ and Ω_{R}, and future experimental investigations should focus on measuring more data points to determine the fundamental scaling relations.

Fig. 3b presents the temperature dependence of the VSC rate constant, plotting $\ln(k/T)$ as a function of $1/T$, for reactions outside the cavity (black) and inside a resonant cavity under various light-matter coupling strengths (colors). If one assumes the rate constant could be described by an Eyring-type equation (transition state theory), then

$$\ln(k/T) \propto -\frac{\Delta H^{\ddagger}}{k_{\mathrm{B}}} \cdot \frac{1}{T} + \frac{\Delta S^{\ddagger}}{k_{\mathrm{B}}}, \tag{19}$$

where the slope is related to $\Delta H^{\ddagger}$ and the y-intercept is related to $\Delta S^{\ddagger}$. The rate constants were obtained from HEOM simulations (filled circles), and fitted by the least square to obtain linearity (thin lines), as well as from FGR rate theory (open circles). One can see that as Ω_{R} increases, both $\Delta H^{\ddagger}$ and $\Delta S^{\ddagger}$ changes. Here, both the HEOM simulation and the FGR rate theory predict the same trend. The previous work based on the classical Grote-Hynes rate theory [16] can only explain the change in $\Delta S^{\ddagger}$. The current FGR-based theory can explain changes in both $\Delta H^{\ddagger}$ and $\Delta S^{\ddagger}$, which has been observed in experiments [1, 4, 6]. Again, we emphasize that the VSC reaction mechanism is *not* related to modification of the $\Delta H^{\ddagger}$ nor $\Delta S^{\ddagger}$, but rather how cavity can mediate vibrational excitations (see Eq. 7) by coupling to $\mathcal{Q}$. However, if one chooses to interpret the change of k/k_0 through the effective changes of $\Delta H^{\ddagger}$ and $\Delta S^{\ddagger}$, then they will exhibit features depicted in Fig. 3b.

Another factor that could influence the VSC-rate constant is the cavity lifetime τ_{c}, which also explicitly shows up in the analytic expression of $\Gamma_{\mathrm{Q}}(\omega)$ (see Eq. 10) and $\tilde{\mathcal{R}}(\omega)$ (see Eq. 12), however, we find that k/k_0 is *not particularly sensitive* to τ_{c}, and the *magnitude* of suppression will be maximized under $\tau_{\mathrm{c}} \to \infty$ limit, but start to converge when $\tau_{\mathrm{c}} \geq 300$ fs (see Supplementary Note 8).

Null VSC results due to low reaction barrier. Recent experimental investigations [70, 71] on CN radical-hydrogen atom abstraction reactions do not reveal any noticeable change in the rate constant, even though the molecular system is under the strong coupling condition. These seemingly null results on the VSC effect will indirectly inform the fundamental mechanism and limitations of the VSC-induced rate constant modifications, and provide insights into when VSC will not be able to change rate constants. As we previously discussed, the reason why cavity is able to modify the rate constant is that $k_1 \ll k_2, k_3$, such that $k \approx k_1$ (see Eq. 7). When the cavity modifies the vibrational excitation rate constant

https://doi.org/10.26434/chemrxiv-2024-m7t4c **ORCID:** https://orcid.org/0000-0002-8639-9299 Content not peer-reviewed by ChemRxiv. **License:** CC BY 4.0

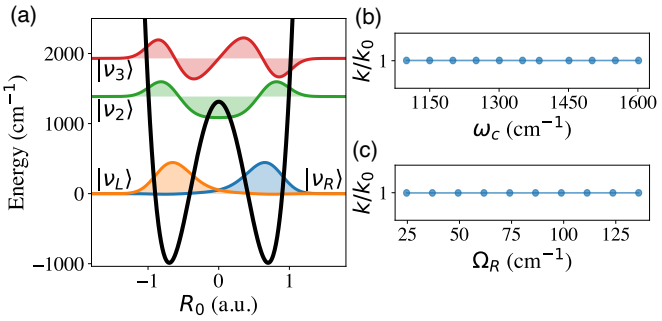

FIG. 4. **Null results of the VSC effects [70, 71] for a reaction that has a low energy barrier.** (**a**) Reaction Potential along the reaction coordinate R_0, with the low reaction barrier [70, 71] such that the vibrational excited states (green and red) are above the barrier, and the mechanistic steps in Eq. 7 are no longer satisfied. k/k_0 at various (**b**) cavity frequencies and (**c**) $\Omega_{\rm R}$, all showing null VSC reactivities.

k_1, this effect manifests into the overall rate of reaction. If the reaction mechanism in Eq. 7 no longer holds, then coupling to the cavity will not modify the rate constant at all. This will indeed be the case when the potential barrier height is even lower than the first vibrational excited state, and ground state tunneling $|\nu_{\rm L}\rangle \rightarrow |\nu_{\rm R}\rangle$ becomes the dominating reactive channel. This is hypothesized to be the case for the CN radical reactions in Ref. 71.

To confirm this hypothesis, we contract a model reactive potential depicted in Fig. 4a with a lower barrier energy $E^{\ddagger}$, such that there is only one localized vibrational state, $|\nu_{\rm L}\rangle$ (orange) in the reactant side as shown in Fig. 4a. The details of the parameters are provided in Supplemental Note 1 (model 2). The first excited state denoted as $|\nu_2\rangle$ (green in Fig. 4a) has a higher energy than the barrier height and is fully delocalized across both reactant and product well. Additionally, the frequency of the spectator mode $\omega_{\rm Q}$ is adjusted to match that of the $|\nu_{\rm L}\rangle \rightarrow |\nu_2\rangle$ transition. Note that one can still achieve VSC when coupling $q_{\rm c}$ with $\mathcal{Q}$ when $\omega_{\rm c} = \omega_{\rm Q}$. This is the minimum model that captures the essential features of the CN radical reactions [70, 71].

Fig. 4b presents the HEOM results of k/k_0 under various cavity frequency $\omega_{\rm c}$ with a strong coupling $\Omega_{\rm R} = 60$ cm^{-1}. We do not observe any noticeable change of k/k_0 over a wide range of cavity frequency, agreeing with the null experimental results in Ref. 71. This is opposed to the situation of Fig. 2c. These results can be interpreted from the vibrational population dynamics provided in Fig. S3 in Supplemental Note 4, where the vibrationally excited states do not actively participate in the forward reaction, and tunneling between $|\nu_{\rm L}\rangle$ and $|\nu_{\rm R}\rangle$ is the primary mechanism leading to the formation of products for this low barrier reaction. Similarly, in Ref. 70, a range of $\Omega_{\rm R}$ were used in the experiments ($25 \leq \Omega_{\rm R} \leq 75$ cm^{-1}), and one still finds null VSC results. Fig. 4c presents k/k_0 under various $\Omega_{\rm R}$ under the resonance condition $\omega_{\rm c} = \omega_{\rm Q}$, and predicts the same null effect. These results suggest that the current theory based on the mechanism in Eq. 7 supports the null VSC results recently discovered in the experiments [70, 71].

As discussed above, we have seen two main mechanisms by which chemical reactions can proceed in our model system : (**a**) the initial vibrational excitation as the limiting reaction step (as described by Eq. 7) and (**b**) the direct tunneling from reactants to products as the main reactive pathway. Whether a reaction proceeds by the first or second mechanism is dictated by the position of the reaction barrier and the conditions are $E_{\rm I}^{\ddagger} > \omega_0$ (for case a) or $E_{\rm II}^{\ddagger} < \omega_0$ (for case b), respectively. Thus, we propose that for two chemically similar reactions only the one obeying mechanism (**a**) will be modified by the VSC effects. Experimental measurements [72] of the barrier height $E^{\ddagger}$ based on infrared absorption spectroscopy (in conjunction with DFT simulations) suggest that (I) alcoholysis reaction between phenylisocyanate and cyclohexanol has a $E_{\rm I}^{\ddagger} = 6.7$ kcal/mol (2343 cm^{-1}), and for a similar alcoholysis reaction (II) between 2,4-toluene-diisocyanate and chloraldhydrate, the activation energy is $E_{\rm II}^{\ddagger} = 2.8$ kcal/mol (973 cm^{-1}). Interestingly, $E_{\rm I}^{\ddagger} > \{\omega_0,\ \omega_{\rm Q}\} > E_{\rm II}^{\ddagger}$, and reaction (I) has been investigated by Simpkins *et al* [10] in a cavity under VSC and found a sharpe resonance suppression (similar to Fig. 2c). The current theory thus predicts that coupling reaction (II) to the cavity will give null results (similar to Fig. 4) due to its low barrier. Future experiments are encouraged to test this theoretical prediction.

Collective Coupling Effect. The current theory $k_{\rm VSC}$ (Eq. 15) also shows collectiveness of the rate constant modification, originating from the collective coupling between R_0 and $\{\mathcal{Q}_j\}$ through $\hat{H}_{\rm RPV}$ in Eq. 2, and the light-matter couplings between $q_{\rm c}$ and $\{\mathcal{Q}_j\}$ through $\hat{H}_{\rm LM}$ (see Eq. 4). We use the spectral density theory to explore the collective effective effect inherent by the Hamiltonian [29] through the analytic expression of $J_{\rm eff}(\omega)$, with details provided in Supplementary Note 5. We consider that N solvent DOF $\mathcal{Q}_j$ have identical frequency $\omega_{\rm Q}$. When $\mathcal{C}_j$ are identical, and there is no disorder in the light-matter coupling angles, only the polaritonic states show up in $J_{\rm eff}(\omega)$ meaning that the $N-1$ dark states present are completely decoupled from the reaction coordinate and will not affect the rate of reaction. This can also be understood from a normal mode analysis approach [29] shown in Supplementary Note 7. As such, the dark vibrational modes are no longer directly coupled to R_0 and will not influence the rate constant. When there are certain disorders in $\mathcal{C}_j$ and also in $\cos\theta_j$, the dark vibrational modes will have a finite spectral density contribution (see Fig. S5-S6 in Supplementary Note 5), and will gradually diminish the VSC collective effect.

Fig. 5a presents k/k_0 with $N = 10^4$ at various $\Omega_{\rm R}$. The overall collective coupling between $\{\mathcal{Q}_j\}$ and R_0 is kept fixed at $\Lambda = 1.71$ cm^{-1} (see Eq. 3). Note that as $\sqrt{N}$ always pair up with $\eta_{\rm c}$ in $k_{\rm VSC}$, the results are thus identical to the case of $N = 1$ with a much larger $\eta_{\rm c}$. The theory predicts a sharp resonance suppression

https://doi.org/10.26434/chemrxiv-2024-m7t4c ORCID: https://orcid.org/0000-0002-8639-9299 Content not peer-reviewed by ChemRxiv. License: CC BY 4.0

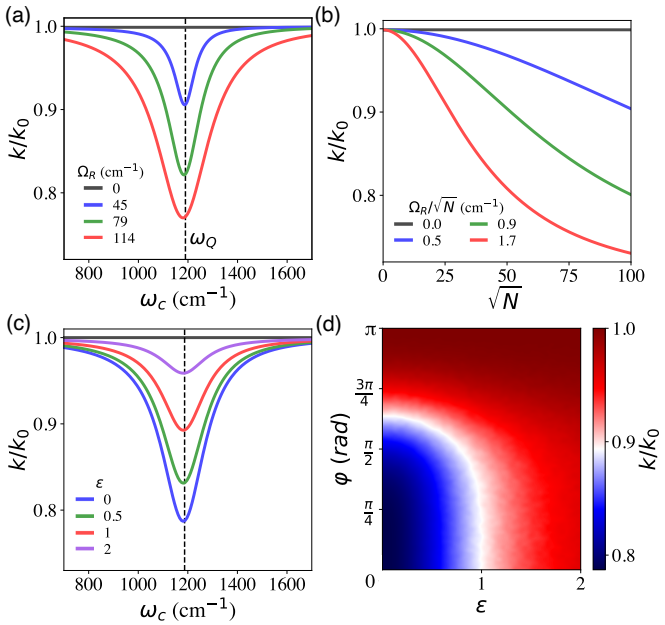

FIG. 5. **Collective Effect predicted by the FGR theory.** (**a**)-(**b**). k/k_0 as a function of (**a**) the cavity frequency under different Ω_{R} and (**b**) numbers of N while the light-matter coupling per molecule η_{c} is kept a constant, with identical $\mathcal{C}_j$ for each vibrational mode. The dipole is assumed to be fully aligned, such that $\chi = 1$. (**c**) k/k_0 as a function of ω_{c}, for a system with $N = 1000$, $\Omega_{\mathrm{R}} = 100$ cm^{-1}, and $\chi = 1$. Here, we consider $\mathcal{C}_j$ disorder, where the couplings $\mathcal{C}_j$ sampled from a normal distribution with standard deviation $\sigma = \varepsilon \cdot 0.1$ cm^{-1}). (**d**) k/k_0 for $N = 1000$, as a function of $\mathcal{C}_j$ disorder ($\sigma = \varepsilon \cdot 0.1$ cm^{-1}) and the angle $\{\varphi_j\}$ between the dipole and cavity polarization, which are sampled from a uniform distribution in the range $\{\varphi_j\} \in [0, \pi]$.

when $\omega_{\mathrm{c}} = \omega_{\mathrm{Q}}$, which can not be captured by previous rate theories [29, 30, 45]. Fig. 5b further present k/k_0 as a function of increasing N, while keeping the light-matter coupling strength $\Omega_{\mathrm{R}}/\sqrt{N}$ constant. The results present the fundamental scaling relation in Eq. 18. Our theory demonstrates the same essential feature of the collective coupling effects observed in the experiments [4], which is the rate constant suppression as increasing the number of molecules (or concentration of the molecules). Under the collective coupling regime, the effect scales as $k_{\mathrm{VSC}} \propto 1/N$ and is caused by the light-matter hybridization induced splitting of $J_{\mathrm{eff}}(\omega)$. It must be emphasized that the values of $\mathcal{C}_j$ depend on the chemical environment of the reactive molecule. One usually expects the solvent-solute coupling involves $N \approx 10^3 - 10^4$ molecules [73–75], which will couple to both R_0 and q_{c}. Note that the light-matter coupling strength per molecule $\eta_{\mathrm{c}} \propto \Omega_{\mathrm{R}}/\sqrt{N}$ used in Fig. 5 is still much larger than the VSC experiments. Future work is required to fully address the collectiveness that emerged from coupling at least $N = 10^6$ molecules to the cavity that leads to the rate constant changes.

Fig. 5c-d further explores the effects of having disorders in $\mathcal{C}_j$, using the exact expression for $J_{\mathrm{eff}}(\omega)$ (see Eq. 34). The exact spectral density under these disorders is presented in Fig. S6 in Supplementary Note 5. Fig. 5c shows the cavity frequency dependence of k/k_0 for $N = 10^3$ at a collective Rabi splitting of $\Omega_{\mathrm{R}} = 100$ cm^{-1}. The values of $\mathcal{C}_j$ are taken from a normal distribution with standard deviation $\sigma = \varepsilon \cdot 0.1$ cm^{-1} where the value of ε will determine the amount of variation in $\mathcal{C}_j$. For all cases considered here, we ensure that Λ is kept constant. Further, there is no angle disorder for the light-matter couplings, such that $\chi = 1$ (c.f. Eq. 11). As one can see, increasing the disorder in the coupling (increasing ε) decreases the cavity effects. This is because adding disorder to the couplings allows the dark states coupling to R_0 to show up in $J_{\mathrm{eff}}(\omega)$ (see Supplementary Note 5, Fig. S6), thus reducing the cavity effect as these dark modes have the same frequency as the vibrations outside the cavity. Nevertheless, the cavity modification effect will survive with a moderate magnitude of disorder, and the fundamental scaling indicated in Eq. 18 is also preserved (see Fig. S6c in Supplementary Note 5). Fig. 5d shows k/k_0 for $N = 1000$ at resonance for several values of ε and $\Omega_{\mathrm{R}} = 100$ cm^{-1}, with both $\mathcal{C}_j$ disorder (satisfies a normal distribution with $\sigma = \varepsilon \cdot 0.1$ cm^{-1}) and the random distribution of the angle between the dipole and cavity field $\{\varphi_j\} \in [0, \varphi]$, with φ changes from 0 (fully ordered) to π (isotropic). One can see that with a small $\mathcal{C}_j$ disorder, the collective VSC effect will survive even for a random disorder of dipole angle for $\{\varphi_j\} \in [0, 3\pi/4]$, due to the fact that the dark modes have a small contribution in the spectral density (see Fig. S5 of Supplementary Note 5). In the previous literature, the conceptual difficulties of explaining the VSC effects are largely due to the densely packed dark states that have the same energy as the original vibrational excitation [20], which will influence the rate constant in the same way outside the cavity. Here, we demonstrate that the extent of the dark states highly depends on the disorder of the system, where the cavity is able to modify the reaction rates even in the presence of such states.

One limitation of the current theory in Eq. 9 is that all VSC effects will vanish for isotropic disordered dipoles if there are no correlations among these angle distributions as for fully isotropically distributed dipoles, $\langle \cos\varphi \rangle = 0$. This is because k_{VSC} explicitly depends on $\chi^2 = \sum_{ij} \cos\varphi_i \cdot \cos\varphi_j / N^2$, and if one assume that $\langle \cos\varphi_i \cdot \cos\varphi_j \rangle = 0$ for $i \neq j$, $\chi^2 = 3/N$. Under these assumptions, χ^2 is negligibly small for a large N, and the VSC effect vanishes in $\Gamma_{\mathrm{Q}}(\omega)$ and $\tilde{\mathcal{R}}(\omega)$ (c.f. Eq. 10 and Eq. 12). Note that Rabi splitting still survives under the isotropic disorder [76], as it only cares about $\langle \cos^2\varphi \rangle = 1/3$, and is expected to be $1/\sqrt{3}$ times smaller than the fully aligned case. Similarly, it is also a great challenge for the previous theories [24, 29, 33] to explain any VSC collective effect when having isotropic disorder for the molecular dipoles. Nevertheless, in real molecular systems, one should expect that $\cos\varphi_i$ and $\cos\varphi_j$ are correlated, at least for neighboring molecules due to the short-range interactions. Further, recent simulations sug-

https://doi.org/10.26434/chemrxiv-2024-m7t4c **ORCID:** https://orcid.org/0000-0002-8639-9299 Content not peer-reviewed by ChemRxiv. **License:** CC BY 4.0

gest that strong light-matter coupling can modify intermolecular interactions and cause alignment of the molecular dipoles [77]. Further theoretical analysis suggests that cavity-induced quantum fluctuations lead to many-body van der Waals interactions, which align intermolecular vectors [78]. All of these theoretical findings suggest that the χ^2 parameter in our theory is not necessarily zero for realistic systems when coupling molecules inside the cavity, and future theoretical investigation is needed to answer this question. Our numerical evaluation of $J_{\text{eff}}(\omega)$ (Eq. 34) also suggests that for a $\{\varphi_j\} \in [0, 3\pi/4]$ isotropic distribution, the dark modes spectral density magnitude is still much smaller than polariton peaks, thus the VSC effects will survive with a moderate angle disorder (see Fig. 5d).

Resonance at the Normal Incidence. The dispersion relation of a FP microcavity [6, 18, 79] is

$$\omega_{\mathbf{k}}(k_{\parallel}) = \frac{c}{n_{\text{c}}}\sqrt{k_{\perp}^2 + k_{\parallel}^2} = \frac{ck_{\perp}}{n_{\text{c}}}\sqrt{1+\tan^2\theta}, \tag{20}$$

where c is the speed of light in vacuum, n_{c} is the refractive index inside the cavity, c/n_{c} is the speed of the light inside the cavity, and θ is the incident angle, which is the angle of the photonic mode wavevector $\mathbf{k}$ relative to the norm direction of the mirrors. For simplicity, we drop n_{c} throughout this paper [80]. The expression of the many-mode Hamiltonian is provided in Supplementary Note 9, Sec. A. When $k_{\parallel} = 0$ (or $\theta = 0$), the photon frequency is

$$\omega_{\text{c}} \equiv \omega_{\mathbf{k}}(k_{\parallel} = 0) = ck_{\perp}, \tag{21}$$

which is the cavity frequency we introduced in Eq. 4. Experimentally, it is observed that only when $\omega_{\text{c}} = \omega_0$ (or at $k_{\parallel} = 0$, $\omega_{\mathbf{k}} = \omega_{\text{Q}}$, known as the normal incidence condition) will there be VSC effects [2, 10, 81]. For a red-detuned cavity ($\omega_{\text{c}} < \omega_{\text{Q}}$), there are still a finite number of modes (with a finite value of $k_{\parallel}$) to fulfill the resonance condition $\omega_{\mathbf{k}} = \omega_0$ and generate polariton states. This is referred to as the oblique incidence, in which one can observe the splitting of the energy levels and the formation of polariton states. Surprisingly, there is no observed VSC effect even though polariton states are formed at a finite $k_{\parallel}$ [2, 6, 10, 17]. Despite recent theoretical progress [82, 83], there is no widely accepted theoretical explanation for the VSC effect which happens only at the normal incidence. Here, we generalize the single mode expression in Eq. 16 into many modes and explain the normal incidence condition. In Supplementary Note 9, we carry out a detailed theoretical analysis. Our results suggest that by considering many modes, the FGR rate constant inside a 1D FP cavity (1-dimension along the $k_{\parallel}$ direction) reduces back to the single mode case, because of the van-Hove-type singularity [84] in the photonic DOS [49]. As a result, inside a 1D FP cavity, VSC modification occurs only at the normal incidence $\omega_{\text{c}} = \omega_0$.

For molecules coupled inside a 2D FP cavity, the FGR rate constant is expressed as follows

$$k_{\text{VSC}}^{\text{2D}} = 2|\Delta_x|^2 \int_0^{\infty} d\omega \, \frac{\Lambda\omega_{\text{Q}}^2 \cdot \omega\Gamma_{\text{Q}}^{\text{2D}}(\omega) \cdot \mathcal{A}_0(\omega-\omega_0)\cdot n(\omega)}{[\omega_{\text{Q}}^2 - \omega^2 + \tilde{\mathcal{R}}^{\text{2D}}(\omega)]^2 + [\omega\Gamma_{\text{Q}}^{\text{2D}}(\omega)]^2}, \tag{22}$$

where $\Gamma_{\text{Q}}^{\text{2D}}(\omega)$ and $\tilde{\mathcal{R}}^{\text{2D}}(\omega)$ are generalized expressions when considering a 2D FP cavity

$$\Gamma_{\text{Q}}^{\text{2D}}(\omega) = \frac{2\lambda_{\text{Q}}}{\gamma_{\text{Q}}} + \int_{\omega_{\text{c}}}^{\infty} d\tilde{\omega} \frac{\mathcal{F}(\tilde{\omega})\cdot N\chi^2\lambda_{\text{c}}^2\tilde{\omega}^2\tau_{\text{c}}^{-1}}{\left(\tilde{\omega}^2-\omega^2\right)^2 + \omega^2\tau_{\text{c}}^{-2}}, \tag{23a}$$

$$\tilde{\mathcal{R}}^{\text{2D}}(\omega) = \int_{\omega_{\text{c}}}^{\infty} d\tilde{\omega} \, \frac{\mathcal{F}(\tilde{\omega})\cdot N\chi^2\lambda_{\text{c}}^2\omega^2}{\left(\tilde{\omega}^2-\omega^2\right)^2 + \omega^2\tau_{\text{c}}^{-2}} \cdot (\omega^2 - \tilde{\omega}^2 + \tau_{\text{c}}^{-2}). \tag{23b}$$

In the above expressions, $\lambda_{\text{c}} = \sqrt{1/(\epsilon_0\mathcal{V})}$ is the cavity frequency independent coupling strength (c.f. Eq. 5), and the weighting factor $\mathcal{F}(\omega)$ is expressed as

$$\mathcal{F}(\omega) = \frac{1}{\mathcal{Z}_{\text{eff}}} \frac{\pi}{(c\Delta k_{\parallel})^2} \cdot \frac{\tau_{\text{c}}^{-1}\omega e^{-\beta\hbar\omega}}{\tau_{\text{c}}^{-1} + \tau_{\parallel}^{-1}(\omega)}, \tag{24}$$

and $\tau_{\parallel}(\omega) = \mathcal{D}\sqrt{k_{\perp}^2 + k_{\parallel}^2}/(c\cdot k_{\parallel}) = \omega\mathcal{D}/\left[c\sqrt{\omega^2-\omega_{\text{c}}^2}\right]$ accounts for the effective photon lifetime due to propagation in the in-plane direction [49] within a mode area with diameter $\mathcal{D}$. Detailed derivations are provided in Supplementary Note 9. The cavity frequency at the normal incidence ($k_{\parallel} = 0$), ω_{c} implicitly shows up in the expressions of $\Gamma_{\text{Q}}^{\text{2D}}$ and $\tilde{\mathcal{R}}^{\text{2D}}$ (see Eqs. 23a-23b) as the lower bound of the $\int d\tilde{\omega}$ integral, due to the photonic DOS only has a finite value when $\omega_{\mathbf{k}} \geq \omega_{\text{c}}$ (or $|k_{\parallel}| \geq 0$).

The rate constant expression $k_{\text{VSC}}^{\text{2D}}$ (Eq. 22) is the **third key result** of this paper. A careful exam of $k_{\text{VSC}}^{\text{2D}}(\omega_{\text{c}})$ in Eq. 22 reveals that the maximum suppression of k/k_0 indeed happenes at the normal incidence. Note that $\mathcal{F}(\omega)$ in Eq. 24 takes a sharp maximum at $k_{\parallel} = 0$ and decays quickly when $k_{\parallel}$ increases, because $\tau_{\parallel}^{-1}$ increases quickly as $k_{\parallel}$ increases [49]. This means that for a 2D cavity, which is used in most VSC experiments, the magnitude of the VSC modification maximizes around $\omega_{\mathbf{k}}(k_{\parallel} = 0) = \omega_{\text{c}} = \omega_{\text{Q}}$, leading to the largest suppression of k/k_0. Eq. 22 thus explains the normal incidence condition for rate constant suppression. Our theory, $k_{\text{VSC}}^{\text{2D}}$ in Eq. 22 thus successfully explains (1) resonance condition, (2) normal incidence condition and operates under the (3) collective coupling regime and (4) thermally activated condition.

Fig. 6 presents the VSC-suppressed rate constant using the FGR expression (Eq. 16) under different Rabi splitting Ω_{R} values and the cavity lifetime is $\tau_{\text{c}} = 500$ fs. Here, we consider the molecule coupled inside (a) a 1D FP cavity and (b) a 2D FP cavity. Fig. 6a presents the results of k/k_0 value using Eq. 16 (dashed line) or numerically evaluating the frequency integral related to the photonic DOS (solid line), see Supplementary Note 9 for

https://doi.org/10.26434/chemrxiv-2024-m7t4c ORCID: https://orcid.org/0000-0002-8639-9299 Content not peer-reviewed by ChemRxiv. License: CC BY 4.0

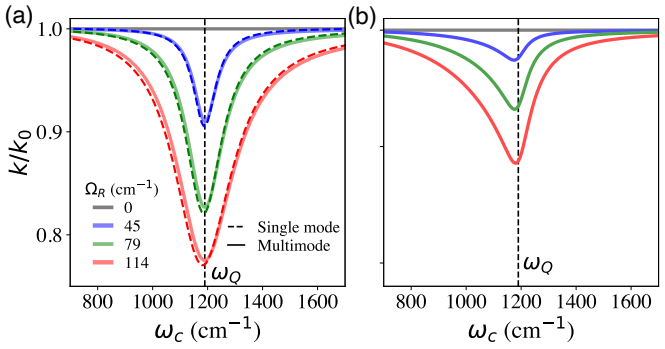

FIG. 6. **Normal Incidence effect for an 1D and 2D FP cavity.** FGR rate profiles of k/k_0 as a function of ω_c, where the cavity lifetime is $\tau_c = 500$ fs. Results under various light-matter coupling strengths are presented. (**a**) FGR rate profiles inside a 1D FP cavity. (**b**) FGR rate profiles for many mode cases inside a 2D FP cavity.

details (numerically evaluate the integral in Eq. S126). The result is visually (near) identical to the single-mode case due to the van-Hove-type singularity in the 1D DOS, depicted in the dashed curve. Fig. 6b presents k/k_0 for many $\mathcal{Q}_j$ DOF coupled to many modes inside a 2D FP cavity, using Eq. 8 with $\alpha = 0.7$, and the $k^{\rm 2D}_{\rm VSC}$ expression in Eq. 22, with the parameter $\mathcal{D} = 3.33\ \mu m$, which is a typical value estimated [49] from the VSC experiments [58]. The numerical integration in Eq. 22 is evaluated using trapezoidal integration, with the numerical details provided in Supplementary Note 9. One can see that the resonance peak is still sharply centered around $\omega_c = \omega_Q$, where ω_c is the normal incidence frequency in a 2D FP cavity. Compared to the single mode or 1D case (Fig. 6a), the k/k_0 distribution is slightly red-shifted, and the resonance peak is asymmetric as it tails toward the lower energy regions ($\omega_c < \omega_0$), which is a prediction form the current theory $k^{\rm 2D}_{\rm VSC}$ (Eq. 22). In recent VSC experiments by Simpkins [10], it does seem that the $\omega_c < \omega_0$ side has a longer tail than the $\omega_c > \omega_0$ side of the action spectrum (see Fig. 3A of Ref. 10). However, this seemingly asymmetrical rate constant profile in Ref. 10 could be caused by a lack of experimental data points for a blue-tuned cavity ($\omega_c > \omega_0$) due to the experimental difficulty of obtaining such measurements. More experimental data are required to test this trend.

To summarize, we present a microscopic mechanism and analytic rate theory that explain resonance VSC suppression of the rate constant under the normal-incidence condition, collective light-matter coupling, and thermally activated regime. In this mechanism, the cavity mode q_c is coupled to the solvent vibrations $\{\mathcal{Q}_j\}$, which in turn coupled to a reaction coordinate R_0. This collective coupling can significantly influence the reaction rate constant of the reaction coordinate. For the model reaction considered in this work, the reactant vibrational excitation $|\nu_{\rm L}\rangle \to |\nu'_{\rm L}\rangle$ is the rate-limiting step and thus controls the overall apparent rate constant. In the current mechanism (Eq. 7), coupling to the cavity explicitly splits the effective solvent spectral density that influences the dynamics of reaction coordinate (see Fig. 2b), and thus reduces the thermal activation rate k_1, hence reducing the overall apparent rate constant.

For a single molecule coupled to a single mode cavity, the theory $k_{\rm VSC}$ (Eq. 16) explains (i) a sharp resonance suppression behavior [1, 10] at $\omega_c = \omega_Q$ (Fig. 2); (ii) non-linear scaling [1, 4] of k/k_0 with respect to Ω_R (Fig. 3a), as well as the non-linear scaling [1, 4] of $\Delta\Delta G^{\ddagger}$ with respect to Ω_R; (iii) modification of both effective activation Entropy and Enthalpy [4] (Fig. 3b). (iv) The null effect [70, 71] because of a very low reaction barrier (Fig. 4), such that the mechanistic in Eq. 7 no longer hold. The analytic theory (using Eq. 8) agrees very well with the numerically exact simulations for all cases.

The theory $k_{\rm VSC}$ (Eq. 16) explains the collective effect, where both the collective solvent-solute coupling Λ as well as the collective light-matter coupling Ω_R show up in the rate constant expression. When there are no disorders for light-matter couplings ($\chi = 1$) and all $\mathcal{Q}_j - R_0$ couplings $\mathcal{C}_j$ are identical, the dark vibrational modes are completely decoupled from R_0, thus not influence the reaction rate constant anymore. We found that a distribution of the $\mathcal{C}_j$ couplings and the angle (φ_j) between the molecular dipole and the cavity field will determine the impact of the dark states on the rate, and the dark vibrational modes will not dominate the spectral density $J_{\rm eff}(\omega)$ with a moderate distribution of $\mathcal{C}_j$ and when the light-matter interaction angles $\{\varphi_j\} \in [0, \pi/4]$ with an isotropic distribution. Beyond that, the magnitude of the dark modes' spectral density dominates over the polariton peaks (see Supplementary Note 5) and the rate constant is reduced back to the outside cavity case (*i.e.*, VSC effect diminished).

Including many cavity modes that obey an FP cavity dispersion, we generalized the theory of $k_{\rm VSC}$ (Eq. 16) to a many-mode version that explains the normal-incidence condition (Fig. 6). This is because, for a 2D FP cavity, the finite in-plane momentum of the mode effectively decreases the effective lifetime of the thermal photon in a given mode volume. This leads to a sharp resonance at $\omega_c = \omega_Q$ when $k_\parallel = 0$. All of the above discoveries bring to a potential first microscopic theory $k^{\rm 2D}_{\rm VSC}$ in Eq. 22, which successfully explains all observed phenomena in VSC experiments so far, including (1) The resonance effect $\omega_c = \omega_Q$, (2) the normal incidence effect, where the VSC effect only happens at $k_\parallel = 0$, and operate under (3) collective coupling condition and (4) the thermal activation regime.

The theory (Eq. 16 or Eq. 22) has several interesting predictions that can be checked experimentally. (a) The magnitude of the VSC effect on rate constant scales (Eq. 18) as Ω_R^2 or N, which should be experimentally verified with more data points that can reliably produce the scaling. (b) For two chemically similar reactions, if one operates under the mechanism in Eq. 7 and satisfies $k_1 \ll k_2, k_3$ but the other does not (due to the low reaction barrier), then the current theory predicts that

https://doi.org/10.26434/chemrxiv-2024-m7t4c **ORCID:** https://orcid.org/0000-0002-8639-9299 Content not peer-reviewed by ChemRxiv. **License:** CC BY 4.0

there will be a VSC effect for the first reaction but not for the second one. (c) Based on $k^{\rm 2D}_{\rm VSC}$ (Eq. 22), the action spectrum should have a longer tail at the red frequency ($\omega_{\rm c} < \omega_{\rm Q}$).

With the current theory, we recommend future experimental investigations to focus on (1) confirming the scaling relation of k/k_0 with respect to $\omega_{\rm R}$ (or N) with more data points. (2) confirming potentially null VSC results in the alcoholysis reaction between 2,4-toluenediisocyanate and chloraldhydrate due to its low barrier [72], which will greatly inform the VSC mechanism, given that the similar alcoholysis reaction between phenylisocyanate and cyclohexanol has shown VSC resonance suppression effects [10]. (3) More data points on the cavity frequency dependence of k/k_0 to provide the shape of the action spectrum , and (4) control the dipole orientations [85, 86] (so one can control χ in Eq. 11) and measure the corresponding VSC effects.

METHODS

Model Hamiltonian. We use a double-well (DW) potential to model the ground state chemical reaction [56, 87]

$$V(\hat{R}) = -\frac{M\omega_{\rm b}^2}{2}\hat{R}^2 + \frac{M^2\omega_{\rm b}^4}{16E^\ddagger}\hat{R}^4, \tag{25}$$

where $M = 1836$ a.u., $\omega_{\rm b} = 1000$ cm^{-1} is the barrier frequency, and $E^\ddagger = 2250$ cm^{-1} is the barrier height. For the matter Hamiltonian $\hat{H}_{\rm M} = \hat{T} + \hat{V}$, the vibrational eigenstates $|\nu_i\rangle$ and eigenenergies E_i are obtained by solving $\hat{H}_{\rm M}|\nu_i\rangle = E_i|\nu_i\rangle$ numerically using the discrete variable representation (sinc-DVR) basis [88] with 1001 grid points in the range of $[-2.5, 2.5]$. To facilitate the mechanistic studies, we diabatize the two lowest eigenstates and obtain two energetically degenerate diabatic states

$$|\nu_{\rm L}\rangle = \frac{1}{\sqrt{2}}\big(|\nu_0\rangle + |\nu_1\rangle\big), \quad |\nu_{\rm R}\rangle = \frac{1}{\sqrt{2}}\big(|\nu_0\rangle - |\nu_1\rangle\big), \tag{26}$$

both with energies of $\mathcal{E} = (E_1+E_0)/2$ and a small tunneling splitting of $\Delta = (E_1-E_0)/2 \approx 1.025$ cm^{-1}. Similarly, for the vibrational excited states $\{|\nu_2\rangle, |\nu_3\rangle\}$, we diabatize them and obtain the first excited *diabatic* vibrational states in the left and right wells as follows

$$|\nu'_{\rm L}\rangle = \frac{1}{\sqrt{2}}\big(|\nu_2\rangle + |\nu_3\rangle\big), \quad |\nu'_{\rm R}\rangle = \frac{1}{\sqrt{2}}\big(|\nu_2\rangle - |\nu_3\rangle\big), \tag{27}$$

with degenerate diabatic energy of $\mathcal{E}' = (E_3+E_2)/2$ and a tunneling splitting of $\Delta' = (E_3 - E_2)/2 \approx 47.68$ cm^{-1}. A schematic representation of these diabatic states is provided in Fig. 1d. Based on the two diabatic states $|\nu_{\rm L}\rangle$ and $|\nu'_{\rm L}\rangle$ in the left well, we define the quantum vibration frequency of the reactant as

$$\omega_0 \equiv \mathcal{E}' - \mathcal{E} = 1189.7 \text{ cm}^{-1}, \tag{28}$$

which is directly related to the quantum transition of $|\nu_{\rm L}\rangle \to |\nu'_{\rm L}\rangle$.

Further, $\hat{H}_\nu$ in Eq. 1 is the system-bath Hamiltonian where each matter DOF is linearly coupled to a set of dissipative phonon bath modes

$$\begin{aligned}\hat{H}_\nu = &\frac{1}{2}\sum_i \Big[\hat{p}_i^2 + \omega_i^2\Big(\hat{x}_i - \frac{c_i}{\omega_i^2}\hat{R}_0\Big)^2\Big] \\ &+ \frac{1}{2}\sum_{j,\zeta}\Big[\hat{p}_{j,\zeta}^2 + \omega_{j,\zeta}^2\Big(\hat{x}_{j,\zeta} - \frac{c_{j,\zeta}}{\omega_{j,\zeta}^2}\mathcal{Q}_j\Big)^2\Big],\end{aligned} \tag{29}$$

where the frequencies (ω_i, ω_ζ) and couplings (c_i, c_ζ) are defined from the spectral density function as follows

$$J_0(\omega) \equiv \frac{\pi}{2}\sum_i \frac{c_i^2}{\omega_i}\delta(\omega-\omega_i) = \frac{2\lambda_0\gamma_0\omega}{\omega^2+\gamma_0^2}, \tag{30a}$$

$$J_{\rm Q}(\omega) \equiv \frac{\pi}{2}\sum_\zeta \frac{c_\zeta^2}{\omega_\zeta}\delta(\omega-\omega_\zeta) = \frac{2\lambda_{\rm Q}\gamma_{\rm Q}\omega}{\omega^2+\gamma_{\rm Q}^2}. \tag{30b}$$

We use Drude-Lorentz model spectral density, with $\gamma_0 = 200$ cm^{-1}, $\gamma_{\rm Q} = 6000$ cm^{-1} for the bath characteristic frequencies and $\lambda_0 = 83.6$ cm^{-1}, $\lambda_{\rm Q} = 0.147$ cm^{-1} for the reorganization energies, similar to the previous work [41].

Finally, the cavity mode interacts with the outside cavity electromagnetic field that acts as a bath for the cavity mode, thus describing the cavity loss

$$\hat{H}_{\rm loss} = \frac{1}{2}\sum_\upsilon \Big[\hat{p}_\upsilon + \omega_\upsilon^2\Big(\hat{x}_\upsilon - \frac{c_\upsilon}{\omega_\upsilon^2}\hat{q}_{\rm c}\Big)^2\Big], \tag{31}$$

where the couplings (c_υ) and frequencies (ω_υ) are sample from the photon-loss bath spectral density $J_{\rm loss}(\omega) \equiv (\pi/2)\sum_\upsilon (c_\upsilon^2/\omega_\upsilon)\delta(\omega-\omega_\upsilon) = (\omega/\tau_{\rm c})\exp(-\omega/\omega_{\rm m})$, where $\tau_{\rm c}$ is the cavity lifetime [47], and we had assumed that photon loss satisfies strict Ohmic dissipation. In other words, as the cutoff frequency $\omega_{\rm m} \to \infty$, the photon bath dynamics reach the Markovian limit [47, 89]. A detailed discussion can be found in Ref. [47].

Rate Constant Calculations. We use hierarchical equations of motion (HEOM) to simulate the population dynamics and obtain the VSC-modified rate constant, see details in Supplementary Note 1-3. Here, we treat $\hat{H}_{\rm M}$ as the quantum subsystem and represent it using the vibrational eigenstates $\{|\nu_0\rangle, |\nu_1\rangle, ...\}$, and the rest terms in the Hamiltonian are treated as the bath in HEOM, see details in Supplementary Note 2. The population dynamics of the "reactant" is computed as $P_{\mathcal{R}}(t) = {\rm Tr}_{\rm S}[(1-\hat{h})\hat{\rho}_{\rm S}(t)]$, where the trace ${\rm Tr}_{\rm S}$ is performed along the system DOF, and $\hat{h} = h(\hat{R}_0 - R^\ddagger)$ is the Heaviside operator with $R^\ddagger = 0$ as the dividing surface for the model potential $V(\hat{R})$ (in Eq. 25). The forward rate constant is obtained by evaluating [41, 47]

$$k = -\lim_{t\to t_{\rm p}} \frac{\dot{P}_{\mathcal{R}}(t)}{P_{\mathcal{R}}(t) + \chi_{\rm eq}\cdot[P_{\mathcal{R}}(t) - 1]}, \tag{32}$$

https://doi.org/10.26434/chemrxiv-2024-m7t4c **ORCID:** https://orcid.org/0000-0002-8639-9299 Content not peer-reviewed by ChemRxiv. **License:** CC BY 4.0

where $\chi_{\rm eq} \equiv P_{\mathcal{R}}/P_{\mathcal{P}}$ denotes the ratio of equilibrium population between the reactant and product. For the symmetric double potential model considered in this work, $\chi_{\rm eq} = 1$. The limit $t \to t_{\rm p}$ represents that the dynamics have already entered the rate process regime (linear response regime) and $t_{\rm p}$ represents the "plateau time" of the time-dependent rate which is equivalent to a flux-side time correlation function formalism [25, 47]. Details of the simulations are provided in Supplementary Note 3.

For the FGR-based theory, we use the value of the k_0 (outside the cavity rate constant) obtained from the HEOM simulation and report $k/k_0 \approx k_{\rm D}/k_0 + \alpha \cdot k_{\rm VSC}/k_0$, where the $\alpha = 0.7$ is an *ad hoc* re-scaling factor needed to bring the value of FGR rate constant to the consistent range with the HEOM results for outside cavity situation when $\eta_{\rm c} = 0$ It is kept fixed for all the results (and for any finite value of $\eta_{\rm c}$) presented in this work.

General expression for $J_{\rm eff}(\omega)$. We performed a normal mode analysis on the Hamiltonian presented in Eq. 1. This analysis is carried out by performing a Fourier transformed on the classical equations of motion $(\partial H/\partial R_i)$, which are solved to obtain

$$\mathcal{K}(\omega) R_0(\omega) = V'_{\omega}(R_0(\omega)), \tag{33}$$

where $R_0(\omega)$ and $V'_{\omega}(R_0(\omega))$ are the Fourier transformed reaction coordinate and $\partial V(R_0)/\partial R_0$. The effective spectral density is given by the branch cut of $\mathcal{K}(\omega)$ on the complex plane

$$J_{\rm eff}(\omega) = \lim_{\epsilon \to 0^+} {\rm Im}[\mathcal{K}(\omega - i\epsilon)] = {\rm Im}\left[\boldsymbol{\mathcal{C}}^T \boldsymbol{\mathcal{M}}^{-1} \boldsymbol{\mathcal{C}}\right] \tag{34}$$

where $\omega \in \mathbb{R}$, $\boldsymbol{\mathcal{C}}$ is the vector containing the $\mathcal{Q}_j - R_0$ couplings and $\boldsymbol{\mathcal{M}}^{-1}$ is the inverse of the matrix containing the light-matter couplings and bath couplings to the $\{\mathcal{Q}_j\}$ modes, with the following expression

$$\boldsymbol{\mathcal{M}} = \begin{bmatrix} \omega_1^2 + P_1(\omega) + \psi(\omega)\nu_1^2 & \cdots & \psi(\omega)\nu_N\nu_1 \\ \vdots & \ddots & \vdots \\ \psi(\omega)\nu_1\nu_N & \cdots & \omega_N^2 + P_N(\omega) + \psi(\omega)\nu_N^2 \end{bmatrix} \tag{35}$$

where ω_j is the frequency of $\mathcal{Q}_j$, $\nu_j = \sqrt{\frac{2}{\omega_{\rm c}}}\eta_j \cdot \cos\varphi_j$. Finally, $P_j(\omega)$ and $\psi(\omega)$ are associated with the phonon baths of the RPV modes and the cavity loss, respectively, according to

$$P_j(\omega) = -\omega^2 - \frac{2\lambda_{{\rm Q},j}\omega}{\omega + i\gamma_{{\rm Q},j}} \tag{36a}$$

$$\psi(\omega) = \frac{\omega_{\rm c}^2 L(\omega)}{\omega_{\rm c}^2 + L(\omega)} \tag{36b}$$

and $L(\omega) = -\omega^2 - i\tau_{\rm c}^{-1}\omega$. A detailed derivation and numerical evaluation of Eq. 34 are provided in Supplementary Note 5.

DATA AVAILABILITY

The data that support the findings of this work are available at `https://github.com/Smontillo/VSC_Suppression`.

CODE AVAILABILITY

The source code for HEOM used in this study is available at `https://github.com/hou-dao/OpenQuant`. The source code for simulating the FGR rate constants, temperature dependence, and resonance condition at the normal incidence are available at `https://github.com/Smontillo/VSC_Suppression`.

ACKNOWLEDGEMENTS

This work was supported by the Air Force Office of Scientific Research under AFOSR Award No. FA9550-23-1-0438, as well as by the National Science Foundation Award under Grant No. CHE-2244683. W.Y. appreciates the support of the Esther M. Conwell Graduate Fellowship from the University of Rochester. P.H. appreciates the support of the Cottrell Scholar Award (a program by the Research Corporation for Science Advancement). Computing resources were provided by the Center for Integrated Research Computing (CIRC) at the University of Rochester. We appreciate the valuable discussions with Eric Koessler, Arkajit Mandal, Wei Bao, Dave McCamant, and Blake Simpkins.

AUTHOR CONTRIBUTIONS

S. M.V., W.Y., and P.H. designed the research. S. M.V. performed the exact quantum dynamics simulations. S. M.V., W.Y., and P.H. derived the analytic rate constant expressions. S. M.V., W.Y., and P.H. wrote the manuscript.

COMPETING INTERESTS

The authors declare no competing interests.

ADDITIONAL INFORMATION

Supplementary information The online version contains supplementary material available at [url].

Correspondence and requests for materials should be addressed to Pengfei Huo.

https://doi.org/10.26434/chemrxiv-2024-m7t4c **ORCID:** https://orcid.org/0000-0002-8639-9299 Content not peer-reviewed by ChemRxiv. **License:** CC BY 4.0

[1] A. Thomas, J. George, A. Shalabney, M. Dryzhakov, S. J. Varma, J. Moran, T. Chervy, X. Zhong, E. Devaux, C. Genet, J. A. Hutchison, and T. W. Ebbesen, Ground-state chemical reactivity under vibrational coupling to the vacuum electromagnetic field, Angew. Chem. Int. Ed. **55**, 11462 (2016).

[2] A. Thomas, L. Lethuillier-Karl, K. Nagarajan, R. M. A. Vergauwe, J. George, T. Chervy, A. Shalabney, E. Devaux, C. Genet, J. Moran, and T. W. Ebbesen, Tilting a ground-state reactivity landscape by vibrational strong coupling, Science **363**, 615 (2019).

[3] R. M. A. Vergauwe, A. Thomas, K. Nagarajan, A. Shalabney, J. George, T. Chervy, M. Seidel, E. Devaux, V. Torbeev, and T. W. Ebbesen, Modification of enzyme activity by vibrational strong coupling of water, Angew. Chem. Int. Ed. **58**, 15324 (2019).

[4] A. Thomas, A. Jayachandran, L. Lethuillier-Karl, R. M. Vergauwe, K. Nagarajan, E. Devaux, C. Genet, J. Moran, and T. W. Ebbesen, Ground state chemistry under vibrational strong coupling: dependence of thermodynamic parameters on the rabi splitting energy, Nanophotonics **9**, 249 (2020).

[5] K. Hirai, R. Takeda, J. A. Hutchison, and H. Uji-i, Modulation of prins cyclization by vibrational strong coupling, Angew. Chem. Int. Ed. **59**, 5332 (2020).

[6] K. Hirai, J. A. Hutchison, and H. Uji-i, Recent progress in vibropolaritonic chemistry, ChemPlusChem **85**, 1981 (2020).

[7] A. Sau, K. Nagarajan, B. Patrahau, L. Lethuillier-Karl, R. M. A. Vergauwe, A. Thomas, J. Moran, C. Genet, and T. W. Ebbesen, Modifying woodward–hoffmann stereoselectivity under vibrational strong coupling, Angew. Chem. Int. Ed. **60**, 5712 (2021).

[8] K. Nagarajan, A. Thomas, and T. W. Ebbesen, Chemistry under vibrational strong coupling, J. Am. Chem. Soc. **143**, 16877 (2021).

[9] J. Bai, Z. Wang, C. Zhong, S. Hou, J. Lian, Q. Si, F. Gao, and F. Zhang, Vibrational coupling with o–h stretching increases catalytic efficiency of sucrase in fabry–pérot microcavity, Biochem. Biophys. Res. Commun. **652**, 31 (2023).

[10] W. Ahn, J. F. Triana, F. Recabal, F. Herrera, and B. S. Simpkins, Modification of ground-state chemical reactivity via light–matter coherence in infrared cavities, Science **380**, 1165 (2023).

[11] J. Lather, P. Bhatt, A. Thomas, T. W. Ebbesen, and J. George, Cavity catalysis by cooperative vibrational strong coupling of reactant and solvent molecules, Angew. Chem. Int. Ed. **58**, 10635 (2019).

[12] J. Lather and J. George, Improving enzyme catalytic efficiency by co-operative vibrational strong coupling of water, J. Phys. Chem. Lett. **12**, 379 (2020).

[13] H. Hiura and A. Shalabney, Vacuum-field catalysis: Accelerated reactions by vibrational ultra strong coupling, ChemRxiv 10.26434/chemrxiv.7234721.v5 (2021).

[14] J. Lather, A. N. K. Thabassum, J. Singh, and J. George, Cavity catalysis: modifying linear free-energy relationship under cooperative vibrational strong coupling, Chem. Sci. **13**, 195 (2022).

[15] B. S. Simpkins, A. D. Dunkelberger, and I. Vurgaftman, Control, modulation, and analytical descriptions of vibrational strong coupling, Chem. Rev. **123**, 5020 (2023).

[16] X. Li, A. Mandal, and P. Huo, Theory of mode-selective chemistry through polaritonic vibrational strong coupling, J. Phys. Chem. Lett. **12**, 6974 (2021).

[17] J. A. Campos-Gonzalez-Angulo, Y. R. Poh, M. Du, and J. Yuen-Zhou, Swinging between shine and shadow: Theoretical advances on thermally activated vibropolaritonic chemistry, J. Chem. Phys. **158**, 230901 (2023).

[18] A. Mandal, M. A. Taylor, B. M. Weight, E. R. Koessler, X. Li, and P. Huo, Theoretical advances in polariton chemistry and molecular cavity quantum electrodynamics, Chem. Rev. **123**, 9786 (2023).

[19] J. Galego, C. Climent, F. J. Garcia-Vidal, and J. Feist, Cavity casimir-polder forces and their effects in ground-state chemical reactivity, Phys. Rev. X **9**, 021057 (2019).

[20] J. A. Campos-Gonzalez-Angulo, R. F. Ribeiro, and J. Yuen-Zhou, Resonant catalysis of thermally activated chemical reactions with vibrational polaritons, Nat. Commun. **10**, 4685 (2019).

[21] I. Vurgaftman, B. S. Simpkins, A. D. Dunkelberger, and J. C. Owrutsky, Negligible effect of vibrational polaritons on chemical reaction rates via the density of states pathway, J. Phys. Chem. Lett. **11**, 3557 (2020).

[22] T. E. Li, A. Nitzan, and J. E. Subotnik, On the origin of ground-state vacuum-field catalysis: Equilibrium consideration, J. Chem. Phys. **152**, 234107 (2020).

[23] V. P. Zhdanov, Vacuum field in a cavity, light-mediated vibrational coupling, and chemical reactivity, Chem. Phys. **535**, 110767 (2020).

[24] J. A. Campos-Gonzalez-Angulo and J. Yuen-Zhou, Polaritonic normal modes in transition state theory, J. Chem. Phys. **152**, 161101 (2020).

[25] X. Li, A. Mandal, and P. Huo, Cavity frequency-dependent theory for vibrational polariton chemistry, Nat. Commun. **12**, 1315 (2021).

[26] C. Schäfer, J. Flick, E. Ronca, P. Narang, and A. Rubio, Shining light on the microscopic resonant mechanism responsible for cavity-mediated chemical reactivity, Nat. Commun. **13**, 7817 (2021).

[27] T. E. Li, A. Nitzan, and J. E. Subotnik, Collective vibrational strong coupling effects on molecular vibrational relaxation and energy transfer: Numerical insights via cavity molecular dynamics simulations, Angew. Chem. Int. Ed. **60**, 15533 (2021).

[28] T. E. Li, A. Nitzan, and J. E. Subotnik, Polariton relaxation under vibrational strong coupling: Comparing cavity molecular dynamics simulations against fermi's golden rule rate, J. Chem. Phys. **156**, 134106 (2022).

[29] A. Mandal, X. Li, and P. Huo, Theory of vibrational polariton chemistry in the collective coupling regime, J. Chem. Phys. **156**, 014101 (2022).

[30] M. Du and J. Yuen-Zhou, Catalysis by dark states in vibropolaritonic chemistry, Phys. Rev. Lett. **128**, 096001 (2022).

[31] J. P. Philbin, Y. Wang, P. Narang, and W. Dou, Chemical reactions in imperfect cavities: Enhancement, suppression, and resonance, J. Phys. Chem. C **126**, 14908 (2022).

[32] D. S. Wang, T. Neuman, S. F. Yelin, and J. Flick, Cavity-modified unimolecular dissociation reactions via intramolecular vibrational energy redistribution, J. Phys.

https://doi.org/10.26434/chemrxiv-2024-m7t4c **ORCID:** https://orcid.org/0000-0002-8639-9299 Content not peer-reviewed by ChemRxiv. **License:** CC BY 4.0

Chem. Lett. **13**, 3317 (2022).
[33] D. S. Wang, J. Flick, and S. F. Yelin, Chemical reactivity under collective vibrational strong coupling, J. Chem. Phys. **157**, 224304 (2022).
[34] J. Sun and O. Vendrell, Suppression and enhancement of thermal chemical rates in a cavity, J. Phys. Chem. Lett. **13**, 4441 (2022).
[35] E. W. Fischer, J. Anders, and P. Saalfrank, Cavity-altered thermal isomerization rates and dynamical resonant localization in vibro-polaritonic chemistry, J. Chem. Phys. **156**, 154305 (2022).
[36] L. P. Lindoy, A. Mandal, and D. R. Reichman, Resonant cavity modification of ground-state chemical kinetics, J. Phys. Chem. Lett. **13**, 6580 (2022).
[37] S. Mondal, D. S. Wang, and S. Keshavamurthy, Dissociation dynamics of a diatomic molecule in an optical cavity, J. Chem. Phys. **157**, 244109 (2022).
[38] J. Cao, Generalized resonance energy transfer theory: Applications to vibrational energy flow in optical cavities, J. Phys. Chem. Lett. **13**, 10943 (2022).
[39] K. S. U. Kansanen and T. T. Heikkilä, Cavity-induced bifurcation in classical rate theory, arXiv , 10.48550/arXiv.2202.12182 (accessed 2023 (2023).
[40] M. Du, Y. R. Poh, and J. Yuen-Zhou, Vibropolaritonic reaction rates in the collective strong coupling regime: Pollak–grabert–hänggi theory, J. Phys. Chem. C. **127**, 5230 (2023).
[41] L. P. Lindoy, A. Mandal, and D. R. Reichman, Quantum dynamical effects of vibrational strong coupling in chemical reactivity, Nat. Commun. **14**, 2733 (2023).
[42] M. C. Anderson, E. J. Woods, T. P. Fay, D. J. Wales, and D. T. Limmer, On the mechanism of polaritonic rate suppression from quantum transition paths, J. Phys. Chem. Lett. **14**, 6888 (2023).
[43] D. S. Wang and S. F. Yelin, A roadmap toward the theory of vibrational polariton chemistry, ACS Photonics **8**, 2818 (2021).
[44] D. Sidler, M. Ruggenthaler, C. Schäfer, E. Ronca, and A. Rubio, A perspective on ab initio modeling of polaritonic chemistry: The role of non-equilibrium effects and quantum collectivity, J. Chem. Phys. **156**, 230901 (2022).
[45] P.-Y. Yang and J. Cao, Quantum effects in chemical reactions under polaritonic vibrational strong coupling, J. Phys. Chem. Lett. **12**, 9531 (2021).
[46] L. P. Lindoy, A. Mandal, and D. R. Reichman, Investigating the collective nature of cavity-modified chemical kinetics under vibrational strong coupling, Nanophotonics doi:10.1515/nanoph-2024-0026 (2024).
[47] W. Ying and P. Huo, Resonance theory and quantum dynamics simulations of vibrational polariton chemistry, J. Chem. Phys. **159**, 084104 (2023).
[48] D. Hu, W. Ying, and P. Huo, Resonance enhancement of vibrational polariton chemistry obtained from the mixed quantum-classical dynamics simulations, J. Phys. Chem. Lett. **14**, 11208 (2023).
[49] W. Ying, M. Taylor, and P. Huo, Resonance theory of vibrational polariton chemistry at the normal incidence, ChemRxiv 10.26434/chemrxiv-2023-3chzx (2023).
[50] W. Ying and P. Huo, Theory of vibrational strong coupling induced polariton chemistry, ChemRxiv 10.26434/chemrxiv-2024-sl6lt (2024).
[51] M. Piejko, B. Patrahau, K. Joseph, C. Muller, E. Devaux, T. W. Ebbesen, and J. Moran, Solvent polarity under vibrational strong coupling, Journal of the American Chemical Society **145**, 13215 (2023).
[52] T. E. Li, A. Nitzan, and J. E. Subotnik, Collective vibrational strong coupling effects on molecular vibrational relaxation and energy transfer: Numerical insights via cavity molecular dynamics simulations, Angew. Chem. Int. Ed. **60**, 15533 (2021).
[53] M. A. D. Taylor, A. Mandal, W. Zhou, and P. Huo, Resolution of gauge ambiguities in molecular cavity quantum electrodynamics, Phys. Rev. Lett. **125**, 123602 (2020).
[54] D. Antoniou and S. D. Schwartz, Internal enzyme motions as a source of catalytic activity: Rate-promoting vibrations and hydrogen tunneling, The Journal of Physical Chemistry B **105**, 5553 (2001).
[55] J. S. Mincer and S. D. Schwartz, Rate-promoting vibrations and coupled hydrogen–electron transfer reactions in the condensed phase: A model for enzymatic catalysis, The Journal of Chemical Physics **120**, 7755 (2004).
[56] Q. Shi, L. Zhu, and L. Chen, Quantum rate dynamics for proton transfer reaction in a model system: Effect of the rate promoting vibrational mode, J. Chem. Phys. **135**, 044505 (2011).
[57] Y. Chalopin, The physical origin of rate promoting vibrations in enzymes revealed by structural rigidity, Scientific Reports **10**, 10.1038/s41598-020-74439-5 (2020).
[58] A. Shalabney, J. George, J. Hutchison, G. Pupillo, C. Genet, and T. W. Ebbesen, Coherent coupling of molecular resonators with a microcavity mode, Nat. Commun. **6**, 5981 (2015).
[59] J. del Pino, J. Feist, and F. J. Garcia-Vidal, Quantum theory of collective strong coupling of molecular vibrations with a microcavity mode, New J. Phys. **17**, 053040 (2015).
[60] K. H. Hughes, C. D. Christ, and I. Burghardt, Effective-mode representation of non-markovian dynamics: A hierarchical approximation of the spectral density. i. application to single surface dynamics, J. Chem. Phys. **131**, 024109 (2009).
[61] K. H. Hughes, C. D. Christ, and I. Burghardt, Effective-mode representation of non-markovian dynamics: A hierarchical approximation of the spectral density. ii. application to environment-induced nonadiabatic dynamics, J. Chem. Phys. **131**, 124108 (2009).
[62] By assuming the dipole of the effective bath is $\hat{\mu}_{\rm eff} = \sum_m \tilde{c}_m \hat{X}_m$, then the Infrared (IR) spectra of the cavity-plus-spectator modes system is simply expressed as $\mathcal{A}_{\rm Q}(\omega) = J_{\rm eff}(\omega)/(1-e^{-\beta\omega})$, according to the fluctuation-dissipation theorem (FDT) [64, 90]. Thus the dark modes do not contribute to the IR spectra of the RPV modes nor directly coupled to the reaction coordinate.
[63] The system is under the strong coupling condition if $\Omega_{\rm R} \gg \frac{1}{2}\tau_{\rm c}^{-1} + \lambda_{\rm Q}/\gamma_{\rm Q}$.
[64] S. Mukamel, *Principles of Nonlinear Optical Spectroscopy* (Oxford University Press, 1995).
[65] Y. Tanimura, Nonperturbative expansion method for a quantum system coupled to a harmonic-oscillator bath, Phys. Rev. A **41**, 6676 (1990).
[66] Y. Tanimura, Nonperturbative expansion method for a quantum system coupled to a harmonic-oscillator bath, Phys. Rev. A **41**, 6676 (1990).
[67] R.-X. Xu, P. Cui, X.-Q. Li, Y. Mo, and Y. Yan, Exact quantum master equation via the calculus on path integrals, J. Chem. Phys. **122**, 041103 (2005).
[68] R.-X. Xu and Y. Yan, Dynamics of quantum dissipation

https://doi.org/10.26434/chemrxiv-2024-m7t4c **ORCID:** https://orcid.org/0000-0002-8639-9299 Content not peer-reviewed by ChemRxiv. **License:** CC BY 4.0

systems interacting with bosonic canonical bath: Hierarchical equations of motion approach, Phys. Rev. E **75**, 031107 (2007).
[69] A. P. Fidler, L. Chen, A. M. McKillop, and M. L. Weichman, Ultrafast dynamics of cn radical reactions with chloroform solvent under vibrational strong coupling (2023), arXiv:2307.04875 [physics.chem-ph].
[70] L. Chen, A. P. Fidler, A. M. McKillop, and M. L. Weichman, Exploring the impact of vibrational cavity coupling strength on ultrafast cn + c-c6h12 reaction dynamics, Nanophotonics doi:10.1515/nanoph-2023-0747 (2024).
[71] A. P. Fidler, L. Chen, A. M. McKillop, and M. L. Weichman, Ultrafast dynamics of CN radical reactions with chloroform solvent under vibrational strong coupling, The Journal of Chemical Physics **159**, 164302 (2023).
[72] F. Kössl, M. Lisaj, V. Kozicha, K. Heynea, and O. Kühn, Monitoring the alcoholysis of isocyanates with infrared spectroscopy, Chem. Phys. Lett **621**, 41 (2015).
[73] G. Hanna and R. Kapral, Quantum-classical liouville dynamics of nonadiabatic proton transfer, J. Chem. Phys. **122**, 244505 (2005).
[74] T. Yamamoto and W. H. Miller, Path integral evaluation of the quantum instanton rate constant for proton transfer in a polar solvent, J. Chem. Phys. **122**, 044106 (2005).
[75] I. R. Craig, M. Thoss, and H. Wang, Accurate quantum-mechanical rate constants for a linear response azzouzborgis proton transfer model employing the multilayer multiconfiguration time-dependent hartree approach, J. Chem. Phys. **135**, 064504 (2011).
[76] For system with arbitrary φ_j distributions, the Rabi splitting is contracted as $\tilde{\Omega}_{\mathrm{R}} = \Omega_{\mathrm{R}} \cdot \sqrt{\langle \cos^2 \varphi \rangle}$, and the isotropic average of the angles is defined as $\langle \cos^2 \varphi \rangle = \frac{1}{N} \sum_{j=1}^{N} \cos^2 \varphi_j$. For the fully aligned molecule, $\langle \cos^2 \varphi \rangle = 1$, and for the fully isotropic case, $\langle \cos^2 \varphi \rangle = 1/3$. Based on the VSC experiments [59], one can theoretically estimated that $N \approx 10^6 \sim 10^{12}$ that are effectively coupled to each cavity mode [59], and $\Omega_{\mathrm{R}} \approx 100\ \mathrm{cm}^{-1}$ for the typical VSC experiments [4, 10].
[77] J. P. Philbin, T. S. Haugland, T. K. Ghosh, E. Ronca, M. Chen, P. Narang, and H. Koch, Vibropolaritonic reaction rates in the collective strong coupling regime: Pollak–grabert–hänggi theory, J. Phys. Chem. Lett. **14**, 8988 (2023).
[78] J. Cao and E. Pollak, Cavity-induced quantum interference and collective interactions in van der waals systems, arXiv arXiv:2310.12881v1 (2024).
[79] T. E. Li, B. Cui, J. E. Subotnik, and A. Nitzan, Molecular polaritonics: Chemical dynamics under strong light–matter coupling, Annu. Rev. Phys. Chem. **73**, 43–71 (2021).
[80] In most of the VSC experiments, $n_{\mathrm{c}} \approx 1.5$ for the solution used inside the microcavity. Because $n_{\mathrm{c}} \approx 1$, it will not influence the order of the magnitude of our discussion.
[81] T. W. Ebbesen, Hybrid light-matter states in a molecular and material science perspective, Acc. Chem. Res. **49**, 2403 (2016).
[82] I. Vurgaftman, B. S. Simpkins, A. D. Dunkelberger, and J. C. Owrutsky, Comparative analysis of polaritons in bulk, dielectric slabs, and planar cavities with implications for cavity-modified reactivity, J. Chem. Phys. **156**, 034110 (2022).
[83] R. F. Ribeiro, Multimode polariton effects on molecular energy transport and spectral fluctuations, Commun. Chem. **5**, 10.1038/s42004-022-00660-0 (2022).
[84] L. V. Hove, The occurrence of singularities in the elastic frequency distribution of a crystal, Phys. Rev. **89**, 1189 (1953).
[85] M. Hertzog, P. Rudquist, J. A. Hutchison, J. George, T. W. Ebbesen, and K. Börjesson, Voltage-controlled switching of strong light–matter interactions using liquid crystals, Chemistry – A European Journal **23**, 18166 (2017).
[86] G. Stemo, H. Yamada, H. Katsuki, and H. Yanagi, Influence of vibrational strong coupling on an ordered liquid crystal, J. Phys. Chem. B **126**, 9399 (2022).
[87] M. Topaler and N. Makri, Quantum rates for a double well coupled to a dissipative bath: Accurate path integral results and comparison with approximate theories, J. Chem. Phys. **101**, 7500 (1994).
[88] D. T. Colbert and W. H. Miller, A novel discrete variable representation for quantum mechanical reactive scattering via the s-matrix kohn method, J. Chem. Phys. **96**, 1982 (1992).
[89] A. Garg, J. N. Onuchic, and V. Ambegaokar, Effect of friction on electron transfer in biomolecules, J. Chem. Phys. **83**, 4491 (1985).
[90] A. Nitzan, *Chemical Dynamics in Condensed Phases* (Oxford, New York, 2006).

https://doi.org/10.26434/chemrxiv-2024-m7t4c **ORCID:** https://orcid.org/0000-0002-8639-9299 Content not peer-reviewed by ChemRxiv. **License:** CC BY 4.0